9950-1053

Land Mobile Satellite Transmission Measurements at 869 MHz

Selected Results from the Dedicated Stratospheric Balloon Experiment of November 12 and 13, 1984.

by

Wolfhard J. Vogel
Electrical Engineering Research Laboratory
The University of Texas at Austin

A Technical Report submitted to
Jet Propulsion Laboratory
under Contract 956520

March 18, 1985 (Revised April 12, 1985)

1. Introduction

In order to give vehicles travelling in rural areas of the United States access to the telephone network, a Land Mobile Satellite System (LMSS) is being planned. It will involve two-way communication between a satellite in geosynchronous orbit and vehicles equipped with the appropriate transceiver and antenna. The system will most probably operate at frequencies in the 800 MHz range (UHF), although some thought is being given to 1500 MHz (L-band).

Propagation effects are one of the topics that need to be considered for a successful system design. This report describes selected results from a propagation experiment in which satellite transmissions were simulated by placing an 869 MHz and a 1501 Mhz transmitter aboard a stratospheric balloon. The balloon was followed on the ground by a van equipped with receivers and data acquisition equipment capable of creating a permanent record of the variations of the received signal amplitude and phase at the two signal frequencies.

The experiment was conducted on November 12th and 13th, 1984. After the launch of a balloon dedicated to this test from the National Scientific Balloon Facility (NSBF) in Palestine, Texas, the experiment took its path eastward through Louisiana, Mississippi, and into Alabama.

Similar measurements were made previously, in October of 1983 and in January of 1984, by adding an 869 MHz transmitter to the payload of other balloon experiments (*Vogel and Torrence, 1984*, *Vogel and Smith, 1985*), but in those experiments only the 869 MHz amplitude was measured and most of the data were collected at elevation angles below 30°. The data described in the following are more applicable to an LMSS for the continental U.S., because the elevation angles at which the observations were made covered the range from 30° on up. Measurements at low elevation angles are more applicable to Canada and experiments using helicopter-borne transmitters have been reported by *Butterworth and Matt (1983)* and *Huck and Butterworth and Matt (1983)*. Measurements using the ATS-6 satellite have been reported by *Hess (1980)*, but these were mostly made in an urban environment.

The author would like to convey his appreciation for the help he has received in conducting this experiment to the staff at the NSBF, to the LMSS study group at JPL for many suggestions for this report, and to Geoffrey Torrence for building the experiment hardware and, with A. J. Walker, joining on a long trip through the south-eastern United States.

2. Experiment Description

2.1 Transmitters

The airborne instrumentation package consisted of three transmitters and three antennas with a total weight of about 50 kg. The transmitters were mounted in a gondola and the antennas were suspended below the gondola to prevent any blockage (**Fig. 1**). The 2.2 million cubic foot balloon also carried navigation (Omega) and telemetry equipment and several hundred kg of ballast.

A block-diagram of the transmitters is shown in **Figure 2**. The 869 MHz ones were enclosed in a well insulated container. They were electrically independent but coupled thermally. This was to provide both redundancy and a way of managing their temperature in the severe environment at the 32 km float altitude of the balloon: a near vacuum at about -50° C temperature with varying solar heating. The temperature of each transmitter was monitored through telemetry and either one or both could be activated for temperature control. As it turned out, however, only one of the transmitters was ever used, because a thermal equilibrium condition established itself within its normal operating range.

The 1501 Mhz transmitter was furnished by the NSBF. It was narrow-band FM modulated by the balloon's telemetry voice channel. In this experiment it served two functions: (1) as a CW signal source (most of the time) and (2) as a voice transponder (occasionally). The latter feature was used for communication between the van and the balloon facility during the experiment, with the balloon acting as a transponder, receiving from the NSBF or the van at about 150 MHz and retransmitting at L-Band.

The output power at 869 and 1501 MHz was 1/4 and 2 watts, respectively. All transmitting antennas were drooping dipole antennas built to dimensions supplied by JPL. Mounted on a circular ground plane of 1m diameter they produced circularly polarized radiation in an azimuth-symmetric pattern with a broad radiation maximum from about 20° to 60° in elevation.

2.2 Receivers

There were two similar receiver systems in the van. In both, the signal from the balloon transmitter was filtered, amplified, downconverted and finally detected in a quadrature detector. The detector outputs were

recorded on an analog tape recorder, along with the vehicle speed, a voice log, and other relevant information from the control computer.

A block diagram of the 869 MHz system is shown in **Figure 3**. The UHF amplifier chain noise temperature of 68°K determined the sensitivity of the receiver. It was preceded by a low-loss cavity filter preventing out-of-band noise saturation of the receiver. The amplified 869.525 MHz signal was converted to 29.525 MHz, filtered, and fed to the input of a modified ICOM amateur radio receiver. This receiver was of frequency synthesized design and could be tuned in 10 Hz increments. The 455 KHz IF signal from the radio was fed to a quadrature detector built from two double-balanced mixers and a 90° phase shifter. The two detector output voltages, at frequencies between dc and 500 Hz and representing the in-phase and quadrature components of the received signal, were amplified and recorded on FM channels of an analog tape recorder. The unfaded carrier-to-noise ratio of the receiver during the experiment was better than 40 dB. The relative accuracy of the measurements was estimated as better than 0.05 dB and 0.3 degrees for fades less than 10 dB.

The major difference between the UHF and L-Band systems was that at 869 MHz in addition to the drooping dipole two other receiving antennas could be used. These were a microstrip and a heli-bowl antenna, supplied by JPL. These antennas could be rotated in the azimuth plane. Their elevation angle was fixed at about 50°.

The instantaneous dynamic range of the receivers was over 30 dB. A personal computer was used to switch the rf gain of the receivers to keep the signals within the linear range of the signal chain. It also monitored and displayed the status of the experiment in progress and saved this information to the analog tape.

A picture of the van taken just before the launch of the balloon is shown in **Figure 4**. Visible are the radomes covering the antennas mounted to a platform a few inches above the roof of the vehicle. In front is the antenna rotator with the microstrip and heli-bowl antennas, in the center is the 1501 MHZ drooping dipole and in the rear the 869 MHz drooping dipole.

2.3 Operation of the Experiment

The balloon was launched on November 12, 1984 at 16:49 CST from Palestine, Texas. After reaching its float altitude it drifted in an easterly direction at speeds varying between 8 and 35 km/hr. The flight was terminated at 14:36 CST on the next day near Linden, Alabama. For the intervening some twenty hours the UHF and L-Band received signal inphase

and quadrature components were recorded continuously. The van travelled on roads ranging from two lane rural roads to interstate highways, with speeds of up to 90 km/hr, while keeping the elevation angle from the vehicle to the balloon above 30°. Data were obtained at elevation angles up to about 90°. At night the balloon position information relayed by the NSBF over the L-Band transmitter was used for planning the route of the van, during the day the balloon was always visible. A video camera was mounted in the front window of the van for a continuous daytime visual record of the terrain through which the vehicle moved.

The path of the van included, from

Texas: Palestine, Elkhart, Alto, Lufkin, Nacogdoches, Milam; from

Louisiana: Many, Leesville, Alexandria, Pollock, Jena, Ferriday; from

Mississippi: Natchez, Brookhaven, Jackson, Meridian; and from

Alabama: Cuba, and Linden.

2.4 Data Calibration and Analysis Procedure

The receiver system was calibrated by disconnecting the antennas from the receivers and injecting a known amount of power through step attenuators. For each possible rf-gain setting of the receiver a calibration was performed in 5 dB steps at the start and at the end of the experiment. From these data, also recorded on the analog tape recorder, a calibration table was built, relating the receiver voltages to absolute power levels.

The analog tapes were digitized with 12-bit resolution at 1000 samples per second for the inphase and quadrature channels and a lower rate for the speed and rf-gain control voltages. The digitized data were organized into files, each one of which consists of 65 records of 1.024 seconds of data. There are about 1,000 of these files stored on tape cartridges for a total of about 750 Mbytes of data. The a/d converter outputs stored in these files were converted to received power and phase through a sequence of programs, making use of the calibration table. Each record was screened by graphic presentation to avoid contamination of the data base. At the present time all the data have been digitized, but none of the L-Band data have been processed any further. **About 3.5 hours worth of the UHF data, covering 165.58 km of driving, have been converted and screened and are the subject of this report.**

Using a quadrature detector allows one to recover both the signal amplitude and phase. Since the transmitter and the receiver oscillators

were free running, they slowly drifted with respect to each other, resulting in the two detector outputs having a slowly varying offset frequency ω_0. Another cause for a varying frequency offset is a change in Doppler frequency due to a change in the relative velocity between the balloon-borne transmitter and the receiver in the van. Looking at the inphase and quadrature voltages on an x-y display of an oscilloscope shows a picture similar to the upper diagram of **Fig. 5**, where a phasor r rotates at a radial frequency ω_0 and amplitude and phase variations can be seen as changes in the length of r and in the frequency of rotation ω_0.

The received power can of course be calculated from the sum of the squares of the two orthogonal components. To get the phase, calculated as the arc-tangent of the inphase and quadrature component, however, one has to eliminate the frequency offset ω_0, which produces a linear increase or decrease with time of the phase. This is the reason for sampling the data at a fixed rate in time (1kHz) instead of at equidistant points in space (every $1/8^{th}$ wavelength) as in the previous experiment. To determine the offset frequency, a Fast Fourier Transform was performed on one of the two output channels for each 1024 point record. The peak frequency multiplied by the time represents the phase shift due to the difference in frequency. It was added or subtracted from the calculated phase, depending on which output was leading the other. Further, any residual phase sawtooth appearance (**Fig. 5**) due to an error in the estimate of the offset frequency and the 2π ambiguity of the arctangent was eliminated and finally the remaining linear trend in the phase data was removed.

3. Results of the Experiment

3.1 Description of the Data Selected for Presentation

A summary of some of the experimental parameters for the 3.5 hours of data analyzed so far is given in **Table 1**. These data were selected because they were taken during daytime hours with the balloon always visible and because they include the whole spectrum of shadowing situations, from (N) **no shadowing** except that produced by interstate overpasses, to (I) **infrequent shadowing** by roadside trees when the ray from the transmitter occasionally passed through the crowns of trees, to (F) **frequent shadowing** by trees, when the line of sight from the van to the transmitter passed mostly through trees. No claim is made that the proportion of these data (48% of N ,19% of I, 33% of F) is representative of all data collected in this experiment, not to mention a continental U.S.

scenario, but it is believed that they give an accurate account for each of the three classes.

The data were classified for their shadowing during final screening, with an independent judgement being made for each one minute of data. **Group N contains data with blockage only caused by overpasses, group I contains data with less than half of the 1.024 second records of the minute showing any shadowing, and group F contains the minute files for which the majority of the one second records show shadowing effects.** Only data obtained with the drooping dipole receiving antenna were selected at driving speeds from 5 mph up. This selection resulted in 76.88 km (228,629 wavelengths) observed at no shadowing, 31.49 km (91,275 wavelengths) at infrequent shadowing, and 55.21 km (160,043 wavelengths) at frequent shadowing.

Table 1
Some Parameters for the Selected Data
(N=no,I=infrequent,F=frequent shadowing)

Time	Location	Road	Elevation	Shadowing
09:04-12:00	Quentin, MS	US 84	40°	F,N
	Beauregard	US 51	45°	F
	Jackson	IH 55	50°	N
	Bienville	IH 20	45°	N,I,F
13:20-13:50	Kewanee,MS	IH 20	40°	F
	Bellamy,AL	AL 8	30°	F

3.2 A Look at Several One Second Records

A total of 12 seconds of signal level and phase data are shown in **Figures 6** through **8**. They can serve to clarify more of the analysis procedures and help to develop an understanding of propagation effects involved in land mobile satellite transmissions. Some of them will be referred to later during the description of the results from the statistical analysis. The legend in these plots contains the time for identification (115046-11 means the record is the 11th second in the minute file started

at 11:50:46 CST and therefore shows the data from 11:50:57 CST), the speed of the van (in mph), and the estimated absolute received line-of-sight (LOS) power level (in dBm).

The LOS signal level indicated in the figures is the estimated mean power level which would have been received if there was no multi-path interference or shadowing. It was derived for each minute of data by taking the average signal level of the four seconds with the lowest standard deviation during that minute. In order to get a reasonable estimate of the LOS level in the case of the frequent shadowing data, the algorithm was modified to include in the averaging only records with a standard deviation below 1.5 dB. The manual screening of the data showed that even in minutes with heavy shadowing there would be some seconds without blockage. Had that not been the case, then the level would have had to be estimated by choosing reference records from adjacent one minute files. The method appears to produce consistent results and obviates the need for an accurate knowledge of the antenna patterns, transmitted power level, van-to-balloon vector, and line losses.

The amplitude and phase data shown in **Fig. 6a,b**,and **c** are typical for a clear line-of-sight. They were taken while the balloon was at 2:30 o'clock relative to the van with an elevation angle of 40°. The van was travelling east on Interstate Highway 20. Peak-to-peak fluctuations are about 1 dB in one record and 2.5 dB in the other two. The phase fluctuations seem to be proportional to the amplitude fluctuations. 10 to 20° fluctuations are obvious as are about 90° of slowly varying phase due to oscillator drift.

An example of driving under an overpass is shown in **Fig. 6d**. Note that the power scale has been expanded. Assuming that the structure overhead has enough steelmesh to not let the direct signal component pass, the average depth of the fade gives an indication of the scattered signal component strength. It is here about 15 to 20 dB below the direct signal. One could test this part of the record for Rayleigh distribution, but this has not been done. The phase, dashed line, shows slopes of up to about 45 degrees in 1 msec. The shift of over 2.5π in 32 msec is suspect, because it occurs while the signal level is at the bottom of the dynamic range of the receiver.

Shadowing examples of varying severity are given in **Figures 7 a** to **d**. These data were taken after the van left IH20 and started driving on Hwy 80 in Alabama. Trees were very close to the road, in some cases even forming a canopy. In general, when there are amplitude fluctuations, the phase also varies, somewhat in proportion, but on a small scale the two records are not highly correlated. No detailed analysis of this has been made yet. The balloon was at 3 o'clock from the van at 35° elevation.

Finally, the signal while driving under an overpass and the 3 seconds following are shown in **Figures 8 a** to **d**. Again, the balloon was at 3 o'clock from the van at 45° elevation. Remarkable in these pictures is the periodicity of the amplitude. This behavior shows up especially around overpasses, but also to some degree at other times. Note that the beat frequency changes. The effect is noticeable even 75 meters beyond the overpass. Such periodicity and its change can be explained with dominant stationary scatterers producing a reflection which is beating with the direct signal. **Figure 9** presents a hypothetical situation in which a dominant scatterer produces an offset frequency of

$$\Delta f = v/\lambda \{ \cos EL \cos AZ - \cos\beta \} \quad Hz$$

where v is the van speed, λ the wavelength, EL and AZ the angles to the transmitter and β is the angle between the scatterer direction and the van vector. In the frame of a second only β is time varying, causing the observed chirping. As different dominant scatterers come into view, jumps in the beat frequency occur. This kind of frequency beating should be minimized if a medium gain antenna with narrow azimuth beamwidth were used instead of the azimuth-omni-directional drooping dipole antenna.

3.3 Power Distribution Function

The power distribution function for the three classes of fading is shown in **Figure 10**. It may seem odd that the data for the infrequent shadowing class show a better performance at above about 99.5% probability, but this is just a consequence of the fact that there were relatively fewer overpasses producing deep fade events in these data than there were in the non-shadowing data. This result could have been avoided by extracting overpass fades from the non-shadowing data. The results are summarized in **Table 2**.

Table 2
Summary of Power Distribution Results

Fading Class	5dB Probability	Signal Margin Req'd for 90%	95%	99%
N	>99%	1dB	1.2dB	2.5dB
I	>99%	1.7dB	1.8dB	3.4dB
F	84%	6.5dB	9dB	15dB

The sharp knee in the no-fading class is caused by the overpasses which produce most of the excursions of the signal level below about 2 dB from the free space level. These results are consistent with the ones obtained previously (*Vogel and Smith, 1985*). **The fading class here has improved margins by about 3dB compared to the data collected in the 20 to 25° elevation angle range in the previous experiment.**

3.4 Rice Power Probability Density Fitting

The Rice-Nakagami probability density function describes the statistical behavior of a received signal composed of a direct wave and many randomly scattered components. The probability function for the signal power s can be expressed in terms of the ratio K of the direct to the scattered power by

$$p(s) = (1+K) * \exp[-s(1+K)-K] * I_0(2\sqrt{s(1+K)K})$$

where I_0 is the modified Bessel function of order zero. Several of the one second data records and of the one minute data files from the no-fading class have been tested for a Ricean power density. This was done by applying a Chi-Square (χ^2) goodness-of-fit test (*Bendat and Piersol, 1971*) to the measured power density histogram and comparing it to the Rice distribution. The K parameter was allowed to vary in order to find a minimum χ^2 value. Constraints about the minimum number of expected observations per class interval make χ^2, as a function of the parameter K, not have a well behaved derivative, and therefore the minimization could not take advantage of available minimization algorithms, but had to be performed interactively. (This would be even more of a problem with 2 parameter probability density models.)

The results of the goodness-of-fit tests are given in terms of the minimum K value found and its level of significance. The χ^2 goodness-of-fit test measures the deviation of experimental data from a hypothetical distribution. The statistics of this estimate obey the χ^2 distribution and the level of significance is an indication of how far "out on the limb" of the χ^2 density one has to go to make the hypothesis acceptable. A greater level of significance means a higher confidence in the truth of the hypothesis.

Of the 63 one second records of the data obtained starting at 11:51:55, 8 had the hypothesis of a Ricean density accepted at a level of significance of .1 with values for K of 75, 160, 160, 106, 111, 97, 83, and 119. Another 3 records were accepted at the .05 level (85, 80, 94), 3 at the .01 level, and 9 at the .005 level. The density function for all 63 seconds was accepted at the .05 level of significance with K=105. Looking back at **Figures 6 b** and **c** showing two records from that minute, one that passed the test at a level of significance of .1 and one that did not pass at a level greater than .001, it is not obvious that **6b** tested Ricean with K= 111, 5[illegible] did not. Both records have a standard deviation of .133.

The Rice density function for K=2 to 256 in steps of powers of 2 has been plotted in **Figure 11a** and the density function for file 115155 from the **non-shadowing** class has been plotted in **Figure 11b** along with the density function of file 133541 from the **frequent fading** class. Three records of that minute were shown in **Figure 7**. It is generally assumed that the fading superimposes a log-normal distribution. No such tests were performed here.

The only other minute of data for which the X^2 test was performed had K= 112 at a .05 level of significance. The high K values obtained seem to be consistent with the power levels measured during overpass blockage events of 10 to 20 dB below the free space level as shown in **Figures 6d** and **8a**.

3.5 Fade and Non-Fade Durations

For the *frequent-shadowing* minutes and *non-shadowing* minutes the two dimensional histograms of the duration of fade vs. duration of following non-fade event were determined. The duration histograms for fades and non-fades for threshold levels of 1,3,5,7, and 9 dB have been plotted in **Figure 12**. They were obtained from the pair histogram by summation. In the *non-shadowing* class only the 1dB threshold was crossed frequently. The scatter of the non-fade durations at very short durations is due to the sampling interval quantization. For the *frequent-shadowing* class there were many events even at the 9 dB level. Both the fade and non-fade histograms peak at just below one wavelength duration.

A contour plot of the fade/non-fade duration density function for the *frequent-shadowing* class at the 5 dB threshold is shown in **Figure 13**. The durations of the non-fades, i.e. the intervals during which the signal level is greater than 5 dB below the LOS level, are about 10% higher than the durations of the fades. The contour values in the graph give the fraction of

the total 17,309 fade/non-fade pairs which were observed at each duration combination.

The probability that a fade of a certain duration will be followed by a non-fade of at least n times that duration, for n=1,2,4, and 8 has been plotted in **Figure 14** for the 3 and 5 dB level for the **non-shadowing** data and the 5 and 9 dB level for the **frequent-shadowing** data. It may seem surprising that these probabilities decline at increasing fade durations, but can be understood when one considers that the small scale ripple of the signal tends to terminate a fade with a short non-fade and is again followed by a short fade followed by a long non-fade (see for instance in **Fig 7d**). One would have to allow for some hysteresis of the threshold level to keep the ripple from affecting the results in this manner, or use smoothed data. This would of course depend on how the data are to be used. The peaks in the probabilities at high fade durations are due to overpass blockage.

3.6 Power Spectra of the Amplitude and Phase

The normalized power spectra of the logarithmic amplitude and the phase for three of the 63 second files are shown in **Figure 15**. They were derived from averaging over 63 individual spectra each. Two of the spectra were for non-shadowing data. Both show a steep decline in power as expected at about twice the Doppler frequency with the spectrum for the case of the transmitter straight ahead having a slightly higher cut-off frequency than the case of the balloon at 1:30 o'clock from the van.The phase has a higher low frequency content due to the relatively slow variations caused by oscillator instability and van acceleration. The standard deviation of the signal level and the phase was about .4 dB and 15 degrees, respectively.

The spectrum derived for data with frequent shadowing shows an increase in low frequency power caused by the variations of the blockage. The power declines somewhat more steeply at about 100 Hz. In this case the balloon was at 9 o'clock from the van. The standard deviation of the amplitude was 1.95 dB and of the phase was 18 degrees. The reason for the small peak in the phase spectrum at about 250 Hz has not yet been identified.

4. Conclusion

Results from simulated satellite transmission measurements at 869 MHz have been presented. Both the amplitude and phase of the signal were measured. The data show that attenuation by roadside trees can be a limiting factor in systems with a 5 dB fade margin, if 84 % availability is not accceptable. In less extreme environments, however, fading is much less severe. Without fading present, the signal power density function often could be described as Ricean with direct to scattered power ratios of about 100. Phase fluctuations were apparent whenever the signal amplitude fluctuated. A typical value for the phase standard deviation was about 20°. The duration of the fades and non-fades tended to cluster close to one wavelength. The power spectrum of both the amplitude and phase show that most of the fluctuations occur at frequencies below twice the Doppler shift.

Data remaining to be analyzed include the 1501 MHz measurements and the tests involving the alternate receiving antennas at 869 MHz.

References

Bendat J. S. and A. G. Piersol, Random Data: Analysis and Measurement Procedures, Wiley-Interscience, New York, 1971

Butterworth, J. S. and E. E. Matt, "The Characterization of Propagation Effects for Land Mobile Satellite Services," IEE Conference Publication No. 222: Satellite Systems for Mobile Communications and Navigation, 91-94, 1983.

Hess, G. C., "Land-Mobile Satellite Excess Path Loss Measurements," IEEE Transactions on Vehicular Technology, Vol. VT-29, NO. 3, 290-297, 1980.

Huck, R. W., J. S. Butterworth, and E. E. Matt, "Propagation Measurements for Land Mobile Satellite Services," IEEE 33rd Vehicular Technology Conference Record, 265-268, 1983.

Vogel, W. J. and G. W. Torrence, "Measurement Results from a Balloon Experiment Simulating Land Mobile Satellite Transmisssions," MSAT-X Report 101, Jet Propulsion Laboratory, Pasadena, Ca, April 1984

Vogel, W. J. and E. K. Smith, "Propagation Considerations in Land Mobile Satellite Transmissions," MSAT-X Report 105, Jan. 1985

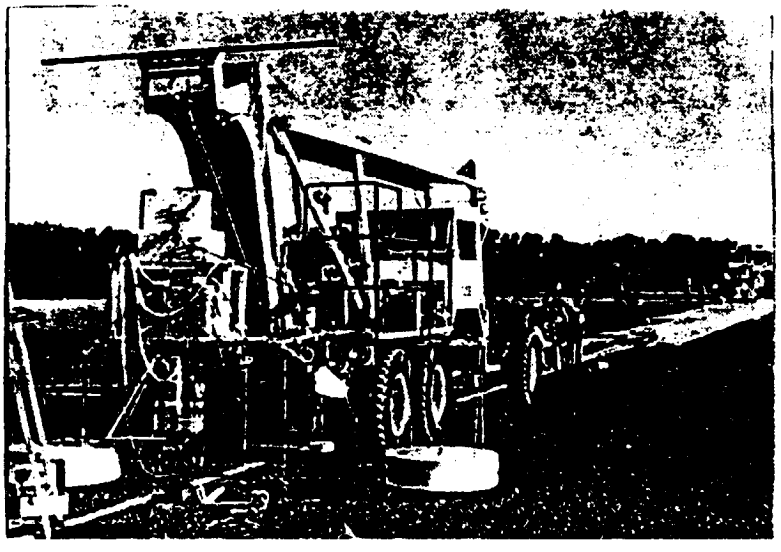

FIG. 1 It takes two large vehicles to launch a balloon and its payload. One holds the balloon while it is being inflated, and the other one holds the instrumentation gondola. After the balloon is released, the vehicle shown drives to keep the connecting lines taut. The payload gets released when the balloon is almost vertically above this vehicle. Visible are the gondola with the transmitters and telemetry equipment and two of the three antennas. The drooping dipoles are protected by polystyrene discs attached to the circular ground planes.

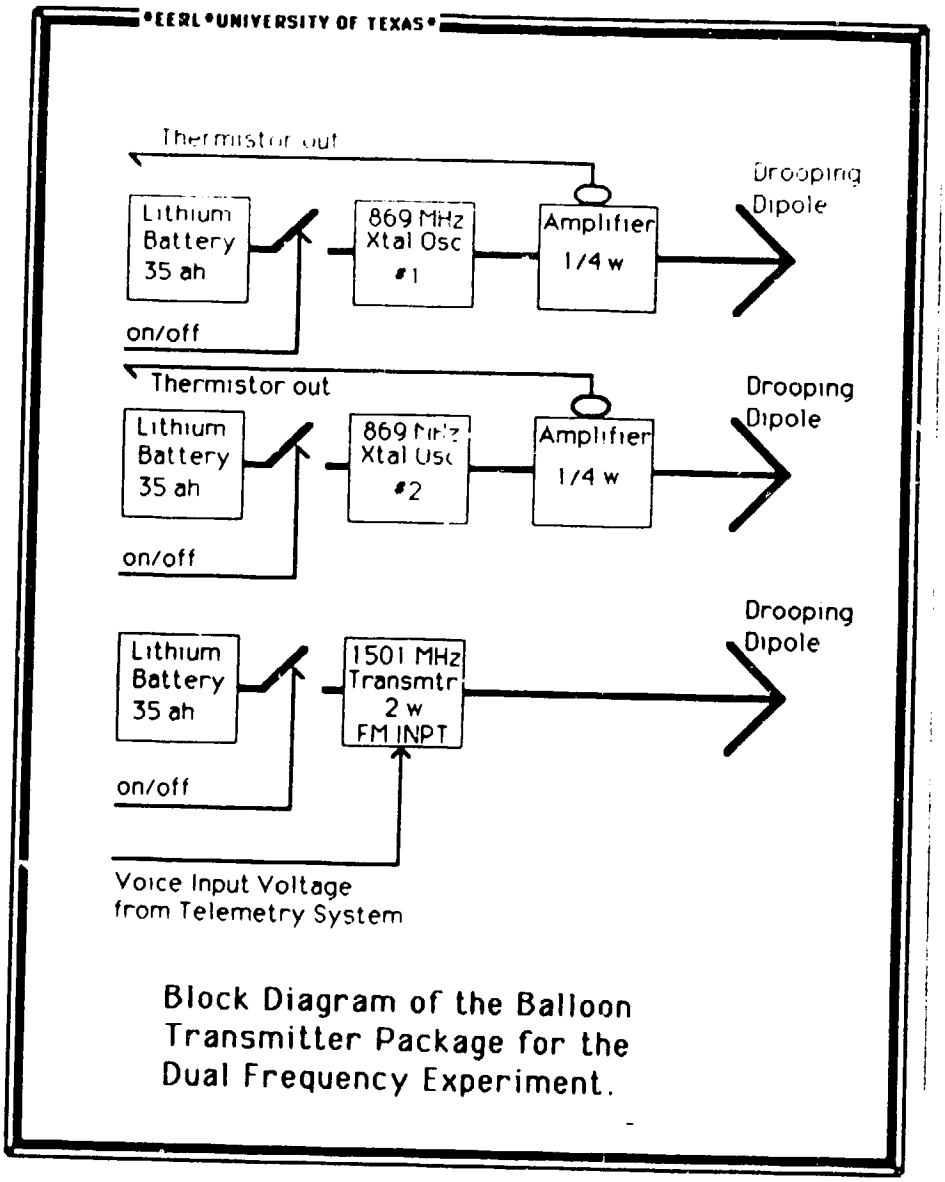

Block Diagram of the Balloon Transmitter Package for the Dual Frequency Experiment.

FIG. 2 The 869 Mhz CW transmitters were enclosed in an insulated box to keep them operating at -50 °C in near vacuum at the 32 km balloon float altitude. There were two transmitters for redundancy. The 1501 MHz transmitter could be FM modulated and was occasionally used for communication from the National Scientific Balloon Facility in Palestine, TX to the driving van. All three transmitters fed drooping dipole antennas.

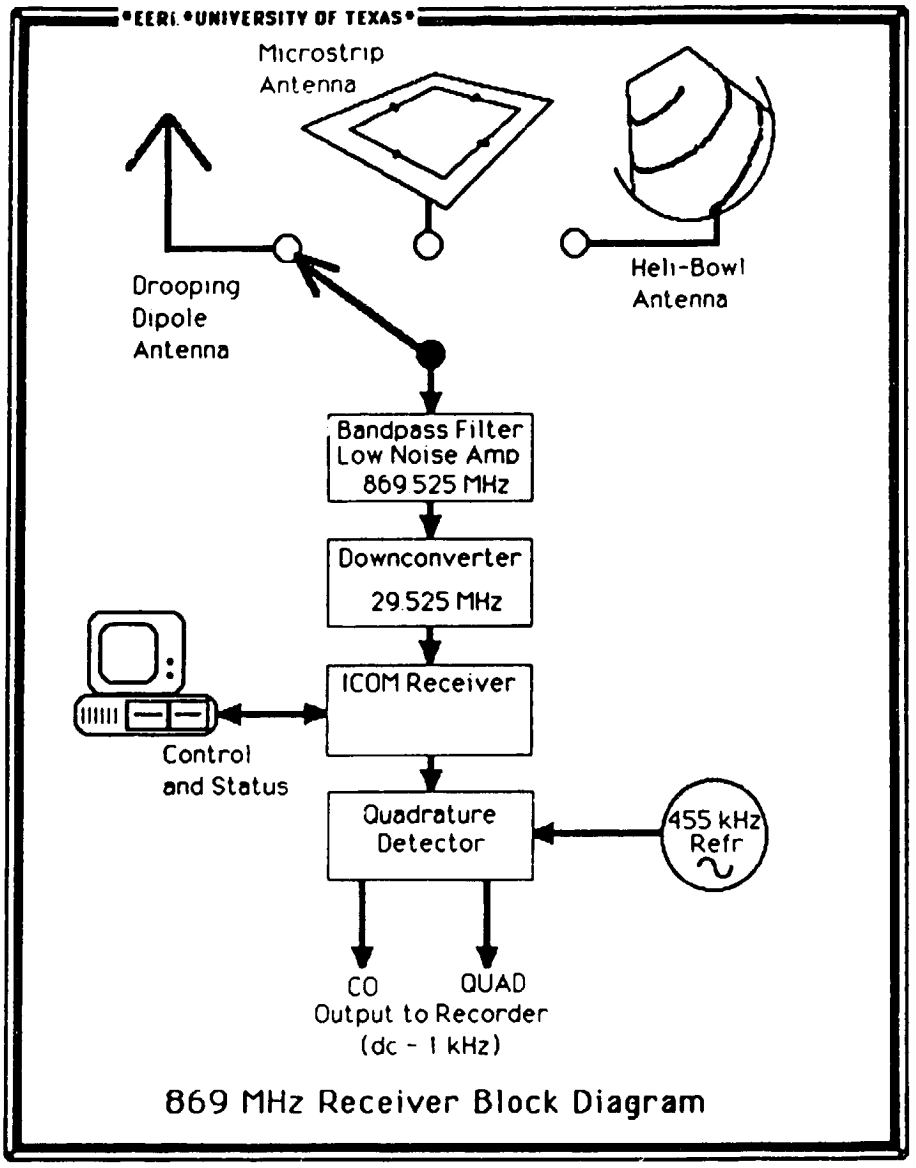

FIG. 3 The 869 MHz receiver used a drooping dipole antenna most of the time, but could also be connected to a microstrip or a heli-bowl antenna. The 68 °K system noise temperature was determined by a low noise FET amplifier. Careful filtering avoided receiver saturation due to noise or out-of-band signals. An amateur radio receiver was the tuneable element in the IF chain. The inphase and quadrature components of the received signal were recorded on analog tape.

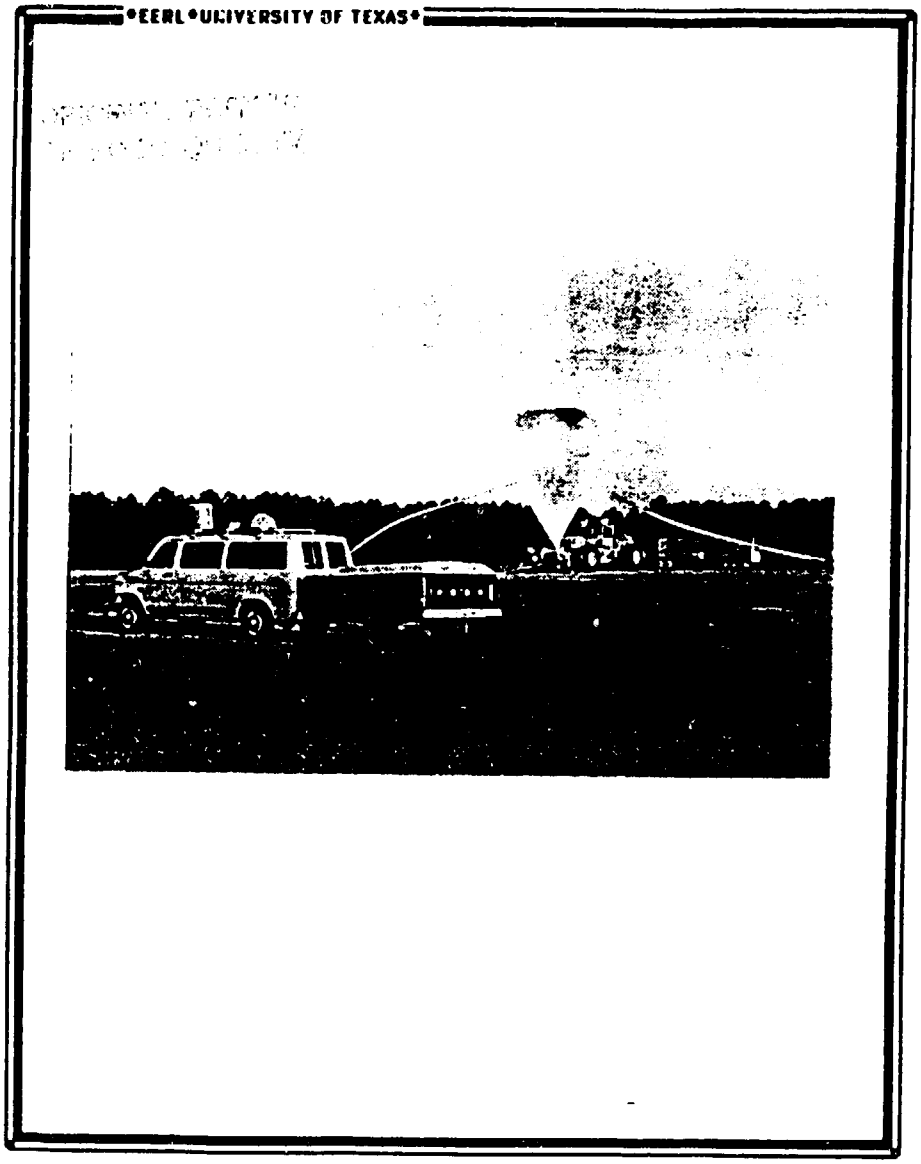

FIG. 4 The PELMOSS van at the launch on 11/12/84. The balloon was almost completely inflated with about 2 million cubic feet of helium. One can see three radomes mounted on top of the van. The front one covered an azimuth positioner with the microstrip and heli-bowl antennas, the center one covered the L-Band drooping dipole antenna, and the rear one covered the UHF drooping dipole.

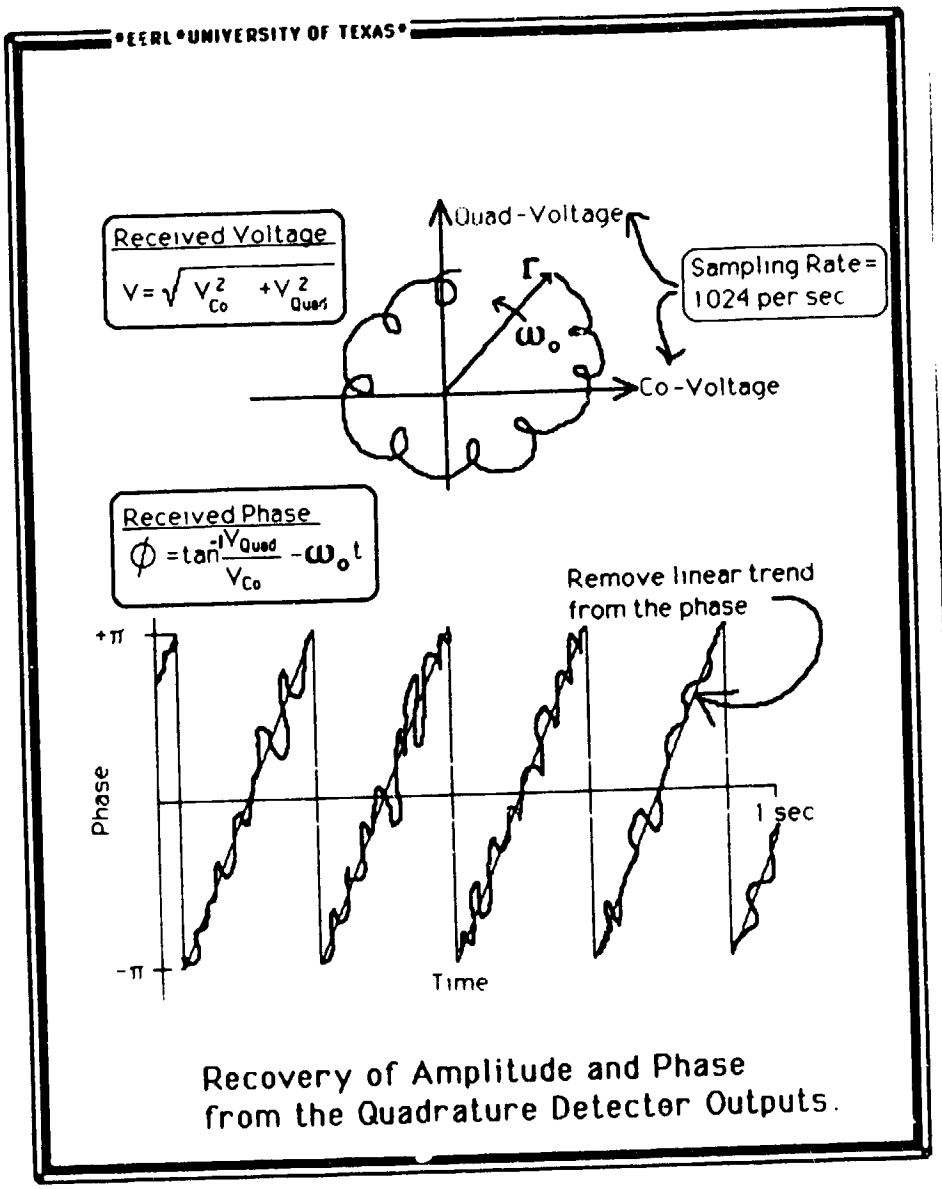

Recovery of Amplitude and Phase from the Quadrature Detector Outputs.

FIG. 5 The transmitter and receiver oscillators were free running. Therefore the output voltage of the quadrature detector was not at dc, but at some slowly varying offset frequency ω_o. To recover the signal phase, one has to subtract the linear trend due to the arbitrary frequency offset and eliminate steps caused by the 2π ambiguity of the arctan function.

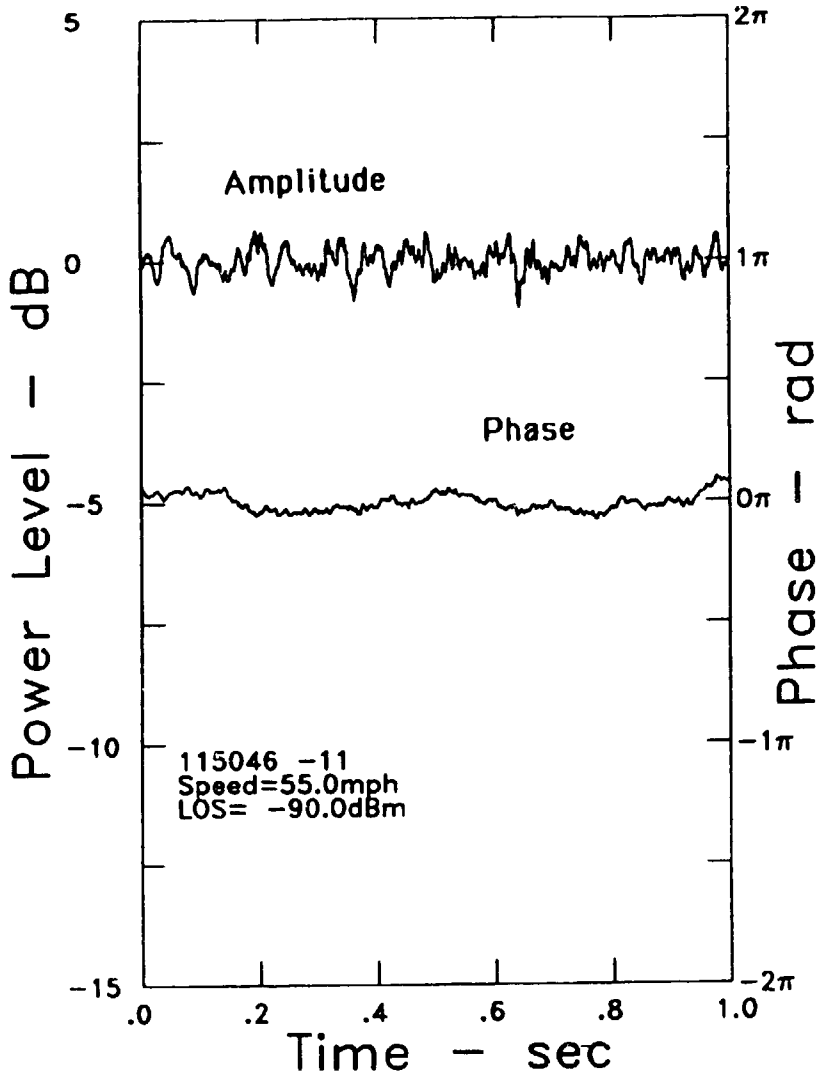

FIG. 6a An examle of the received amplitude and phase. This record was taken at 11:50:57 CST, while the van was driving with a speed of 55 mph on IH 20 in Mississippi. There was no shadowing by trees at this time. Peak-to-peak variations of the amplitude are about 1.5 dB and of the phase about 28 degrees over the second, but less than 10 degrees for the faster variations.

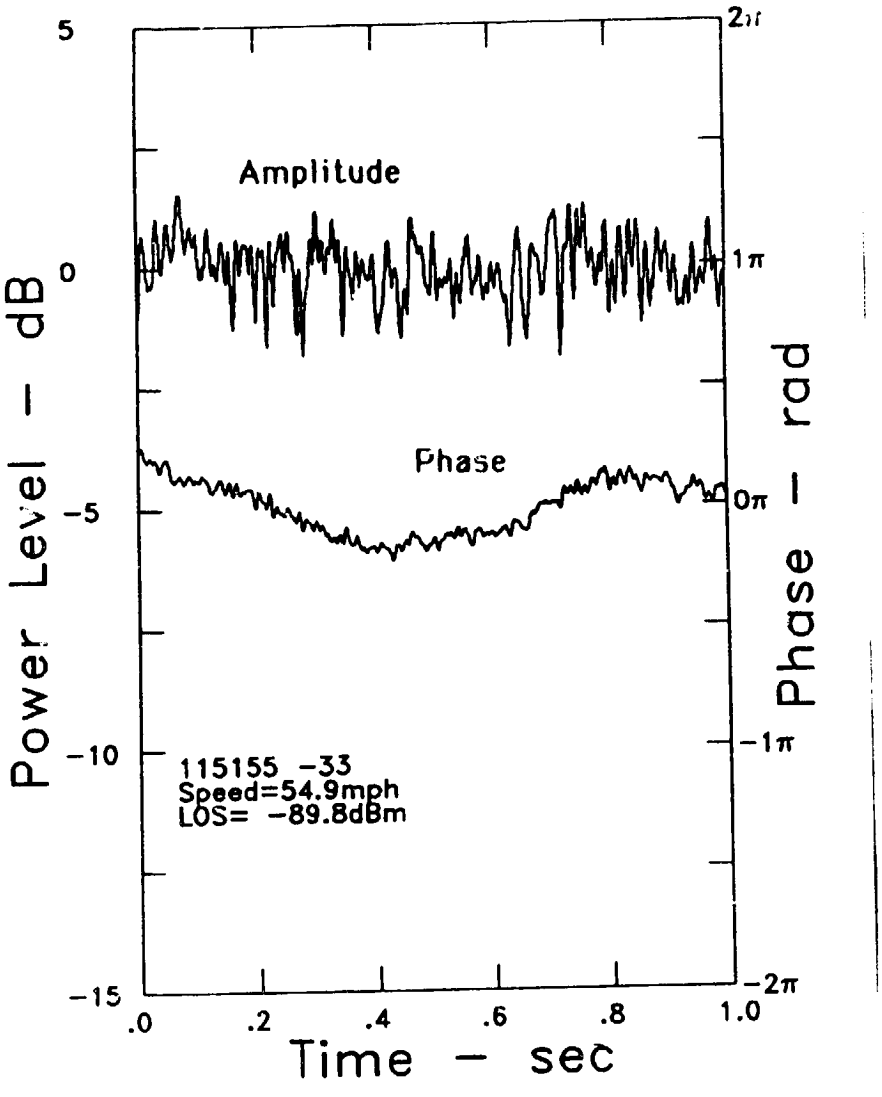

FIG. 6b The record from 11:52:28 CST, also taken on IH20, shows somewhat larger amplitude and phase fluctuations (ptp 3dB, 22°) than the previous one. No shadowing was observed. The low frequency variation of the phase is due to oscillator drift.

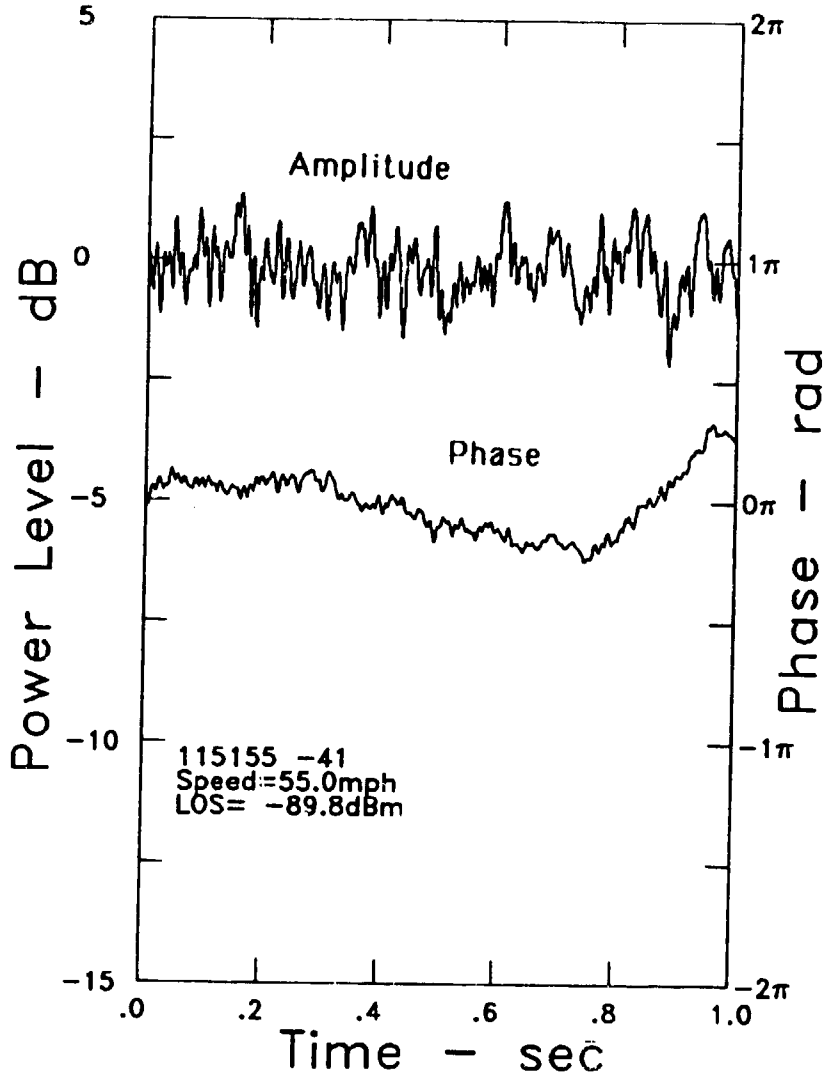

FIG. 6c The data taken at 11:52:36 CST under the same conditions as the ones in Fig. 6b show the apparent consistency of the results.

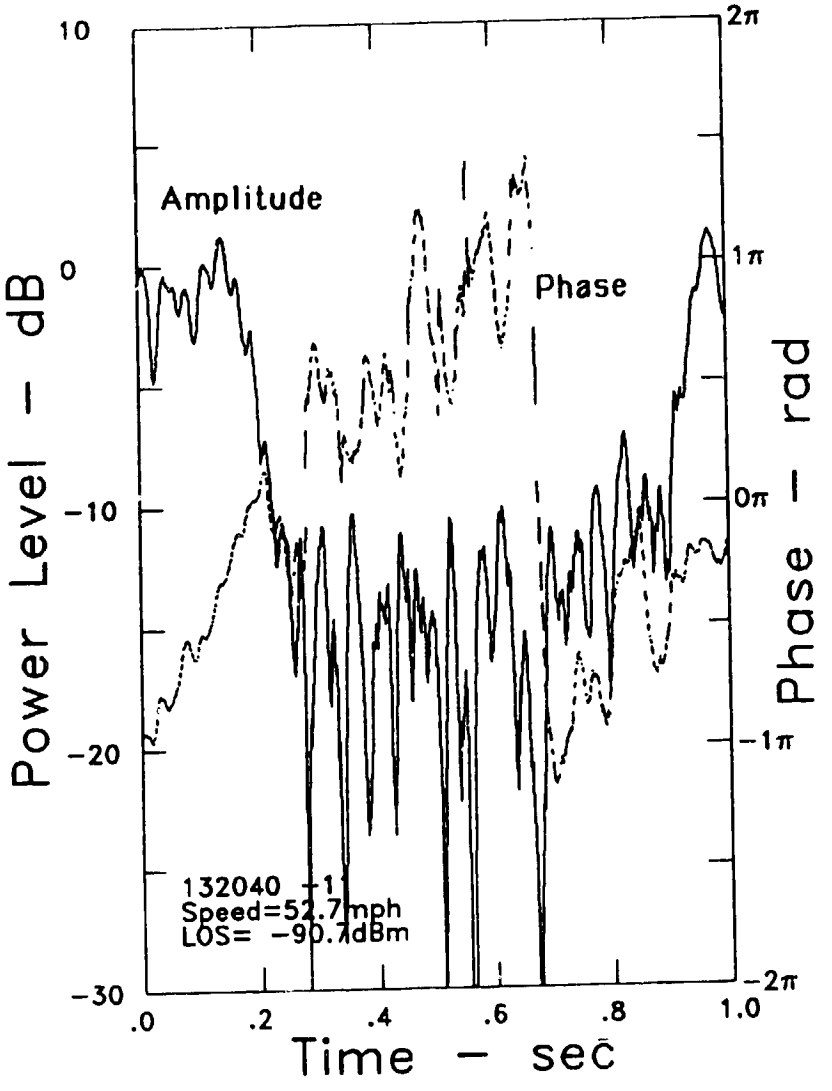

FIG. 6d Driving under an overpass on IH20 probably blocks out most of the direct signal component. What remains is energy scattered from the terrain. The average signal level during the fade is about 15 dB below the LOS level and peak-to-peak variations of about 20 dB are apparent. The phase varies quite rapidly during the fade, but the large jump at .7 sec is suspect, because it ocurred at a signal level close to the bottom of the instantaneous dynamic range of the receiver.

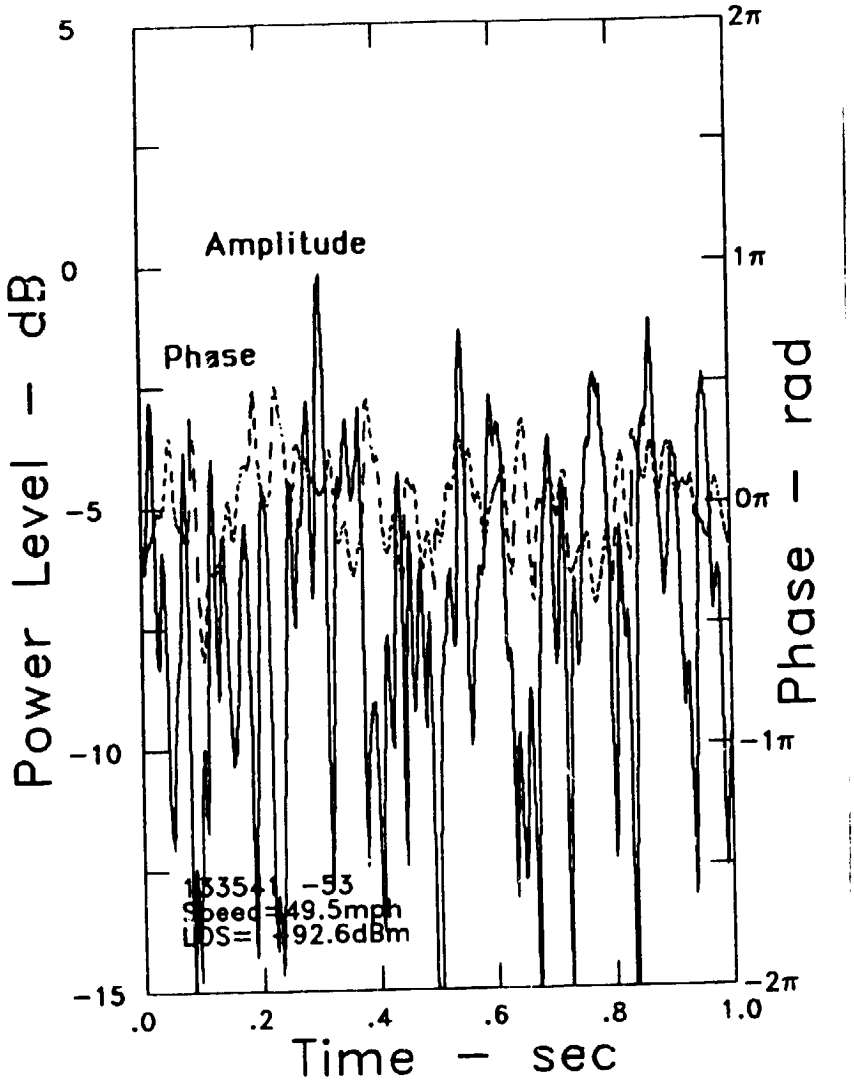

FIG. 7a Shadowing by trees is demonstrated in this figure. The data were taken at 13:36:34 CST on Hwy 80 in Alabama. The angle of elevation to the balloon was 40°. The average signal is about 7.5 dB below the clear LOS level. Peak-to-peak variations are 15 dB and 208°. The LOS level was determined from records close to this one, which were not affected by shadowing.

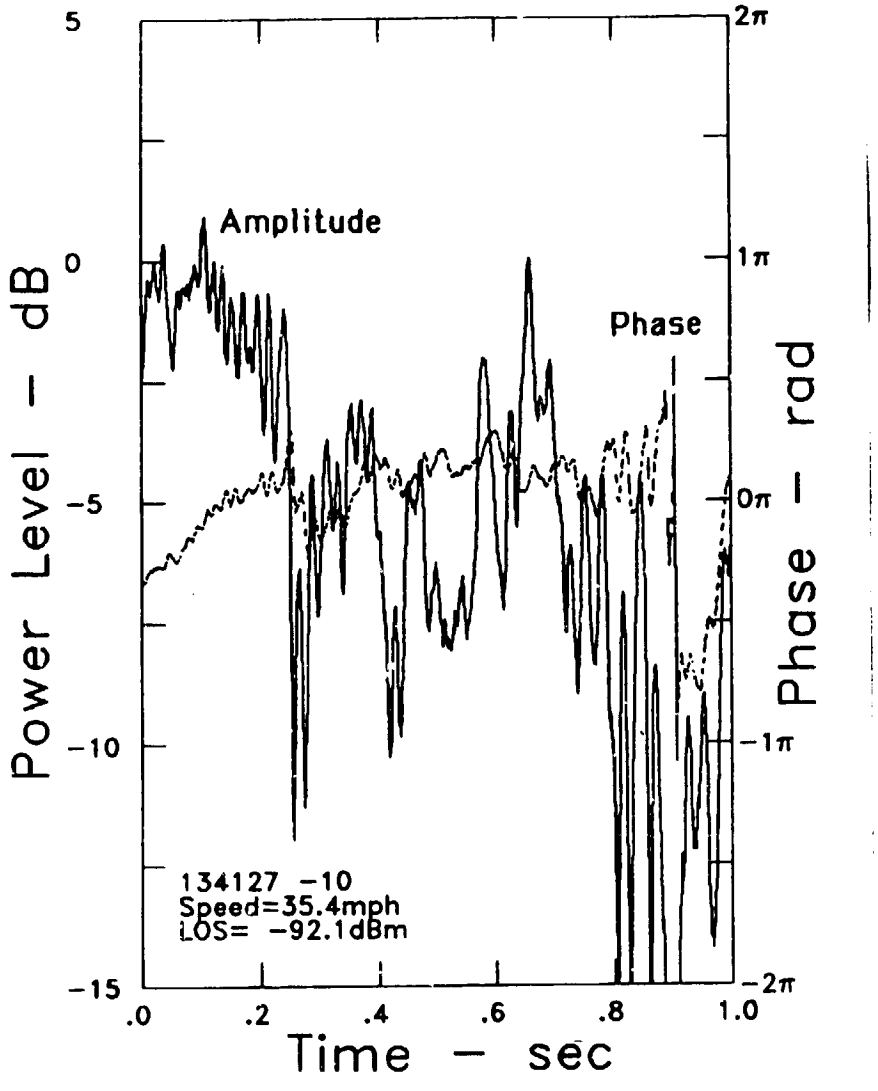

FIG. 7b A less severe example of shadowing by trees, taken about 5 minutes after the previous one. The van speed was 35.4 mph. The balloon was at 3 o'clock from the van at 35° elevation.

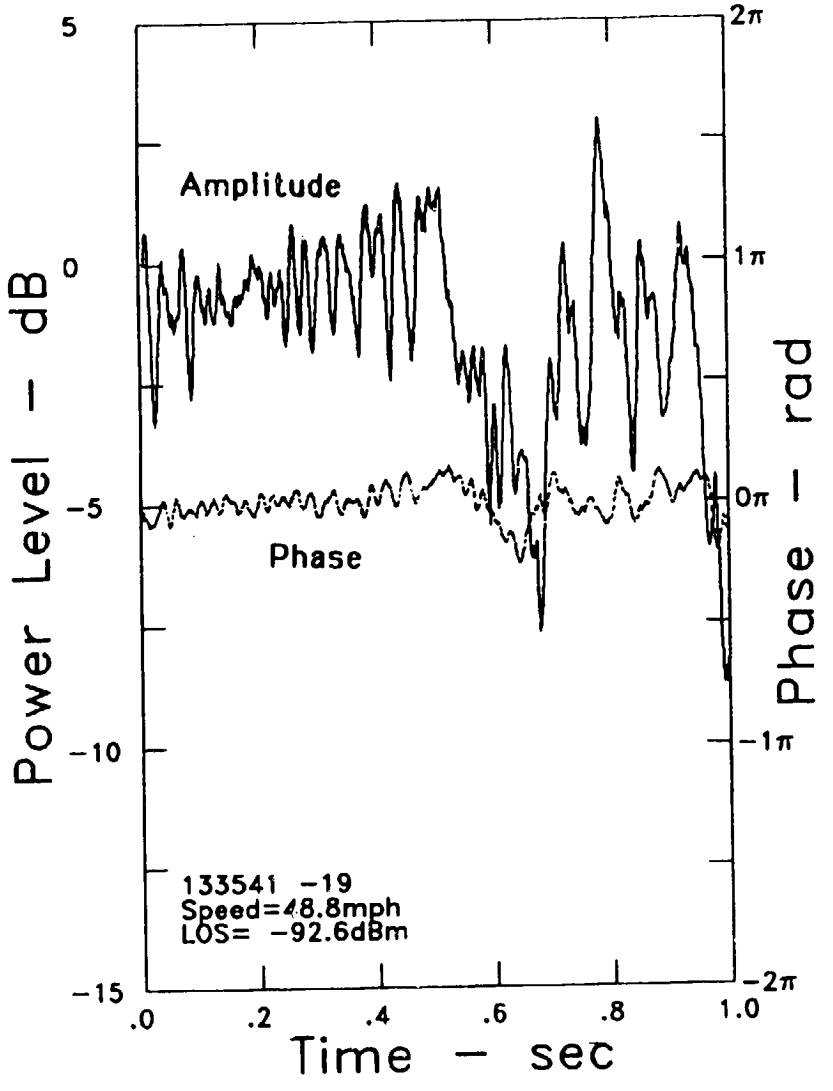

FIG. 7c In this shadowing example 10 dB and 72° peak-to-peak fluctuations were observed. For a short time, the signal was enhanced to about 2.5 dB above the clear LOS level.

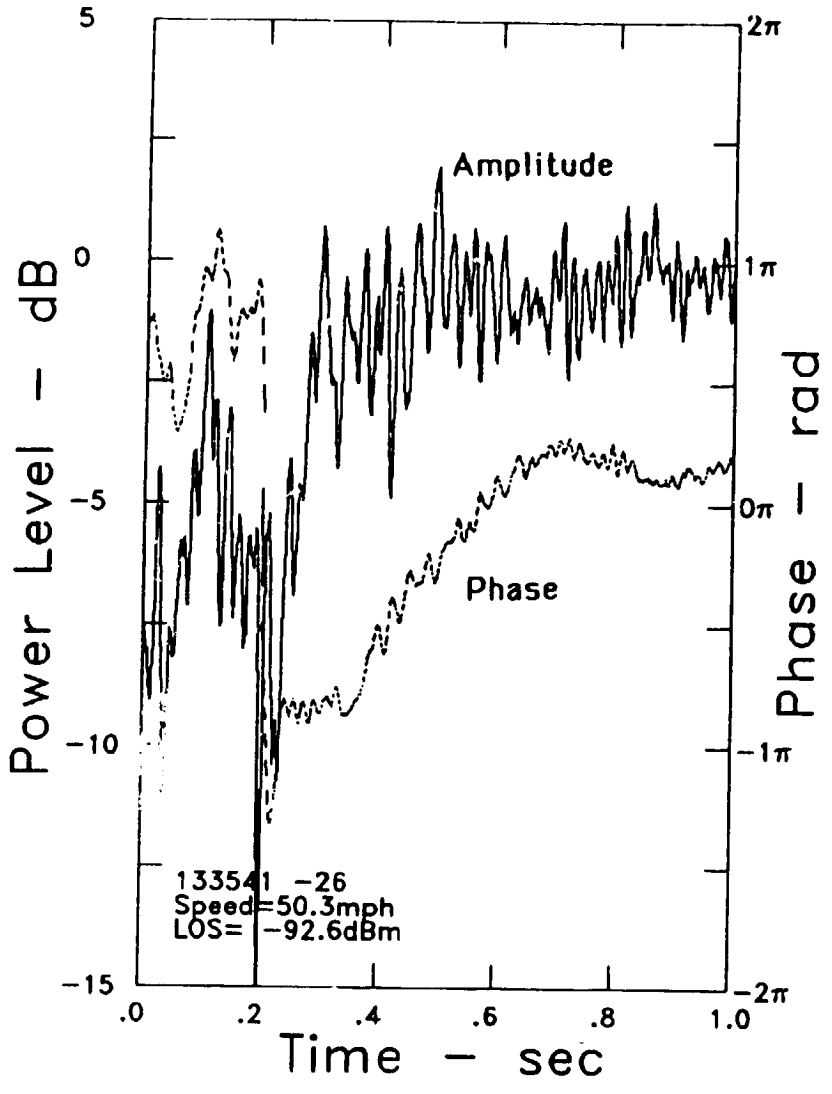

FIG. 7d As the signal recovers from a fade, both the amplitude and the phase fluctuations decrease. On a small scale, the amplitude and the phase do not apppear highly correlated.

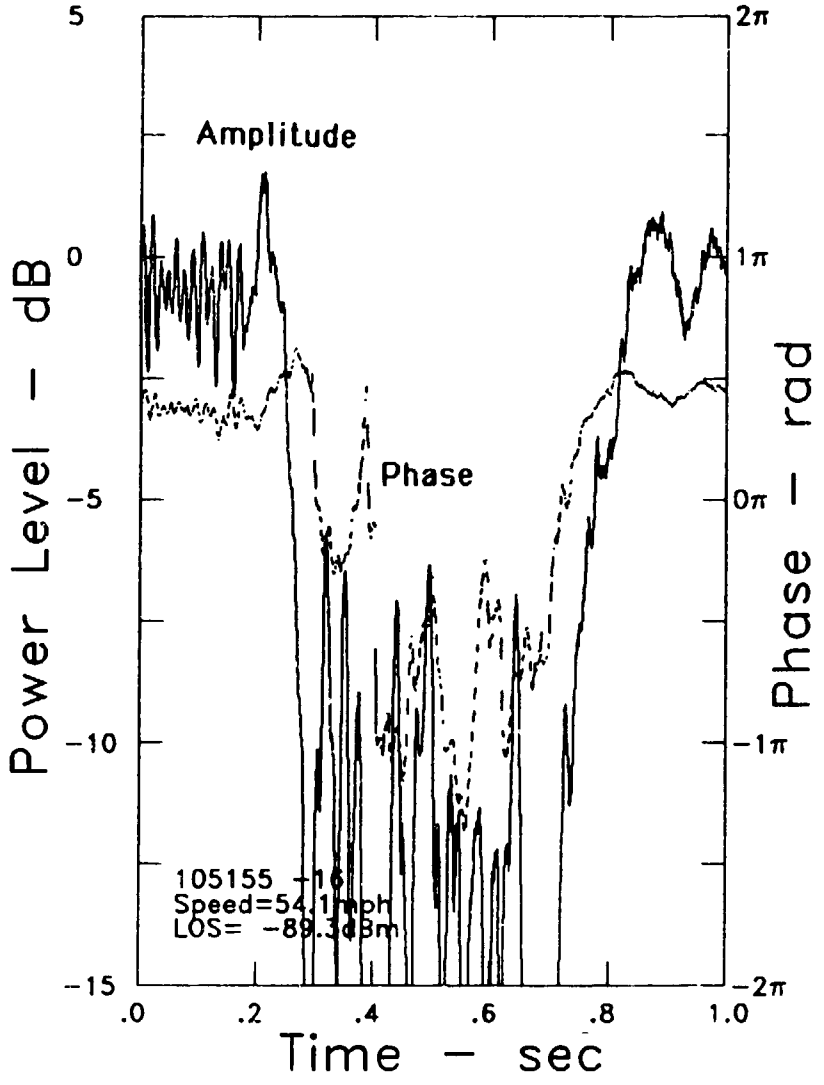

FIG. 8a This figure and the next three have been included to show the typical effect of driving under an overpass. As the line-of sight gets obscured, the signal level first rises, before decreasing by an average of about 15 dB in the shadow of the overhead structure. Emerging from the shadow zone, straight-edge diffraction effects are observed again.

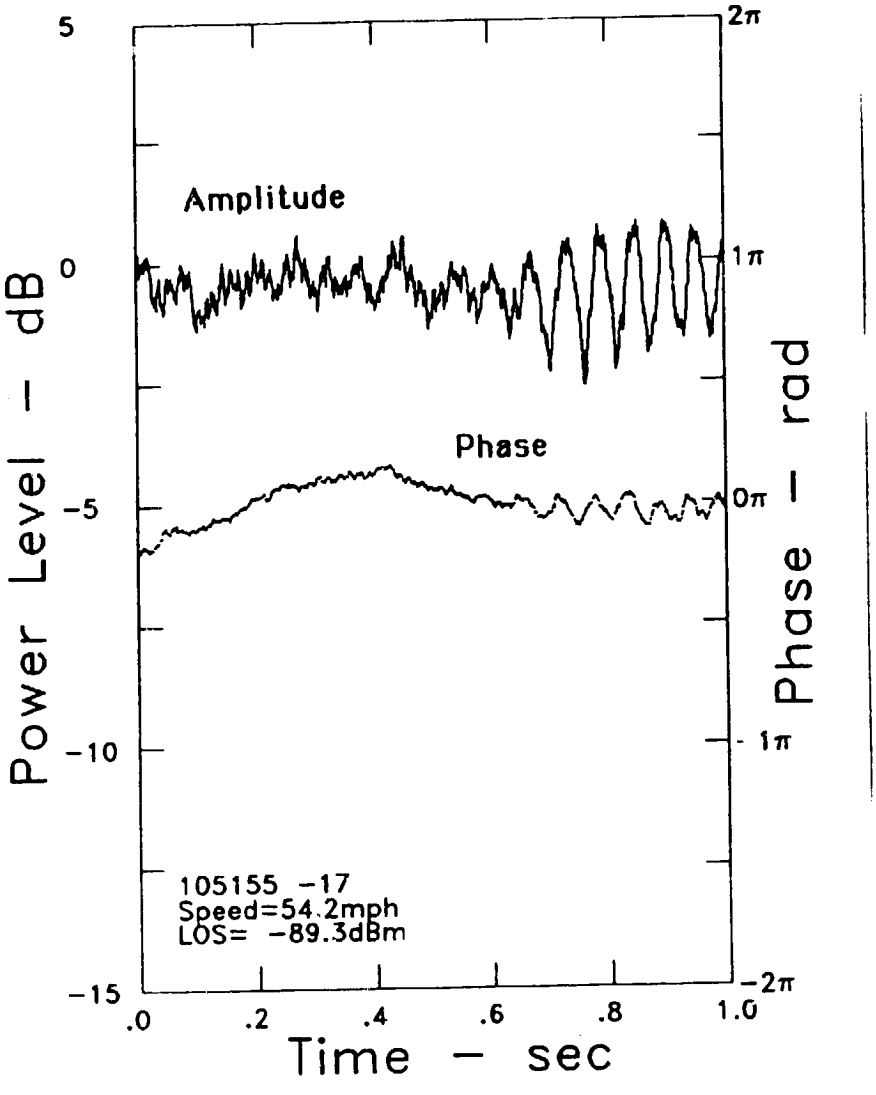

FIG. 8b About 1/2 second after the overpass (or 14 meters) a 3 dB, 30° peak-to-peak beat was observed with a spatial interval of about 3.5λ.

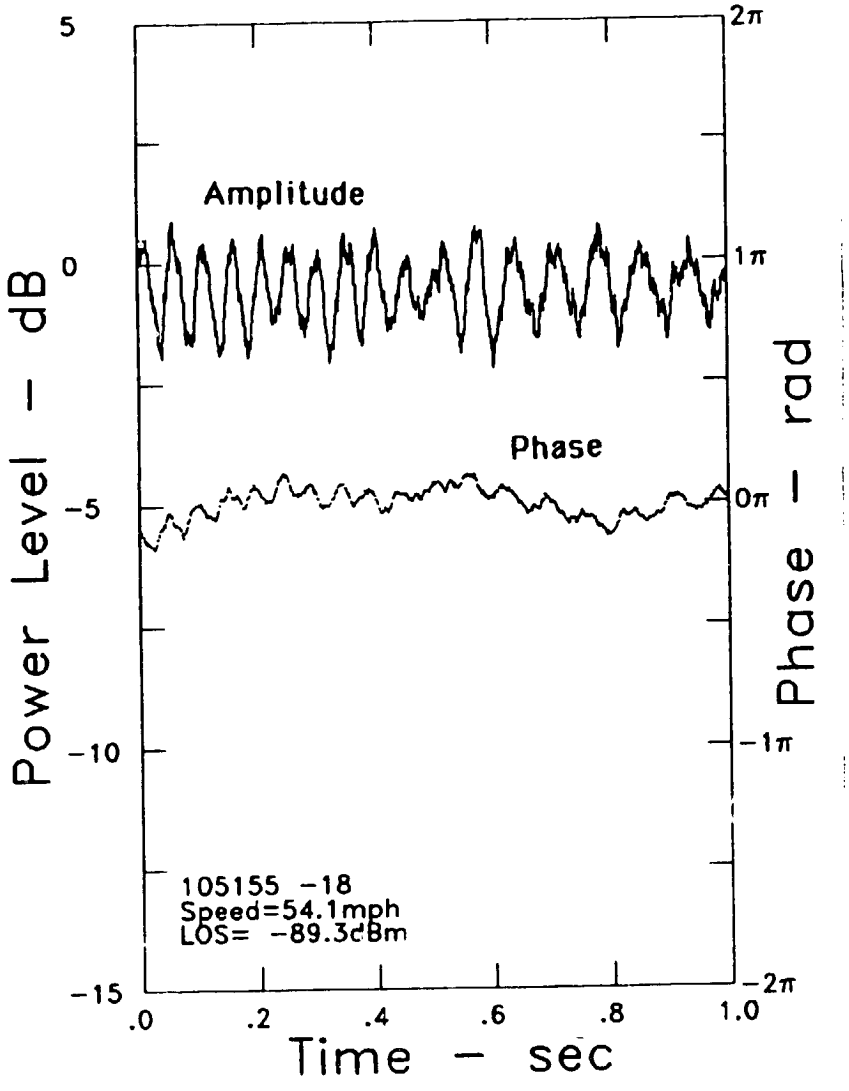

FIG. 8c About 36 meters after the overpass, the beat frequency changed by about 50%. This can be observed both in the amplitude and phase data.

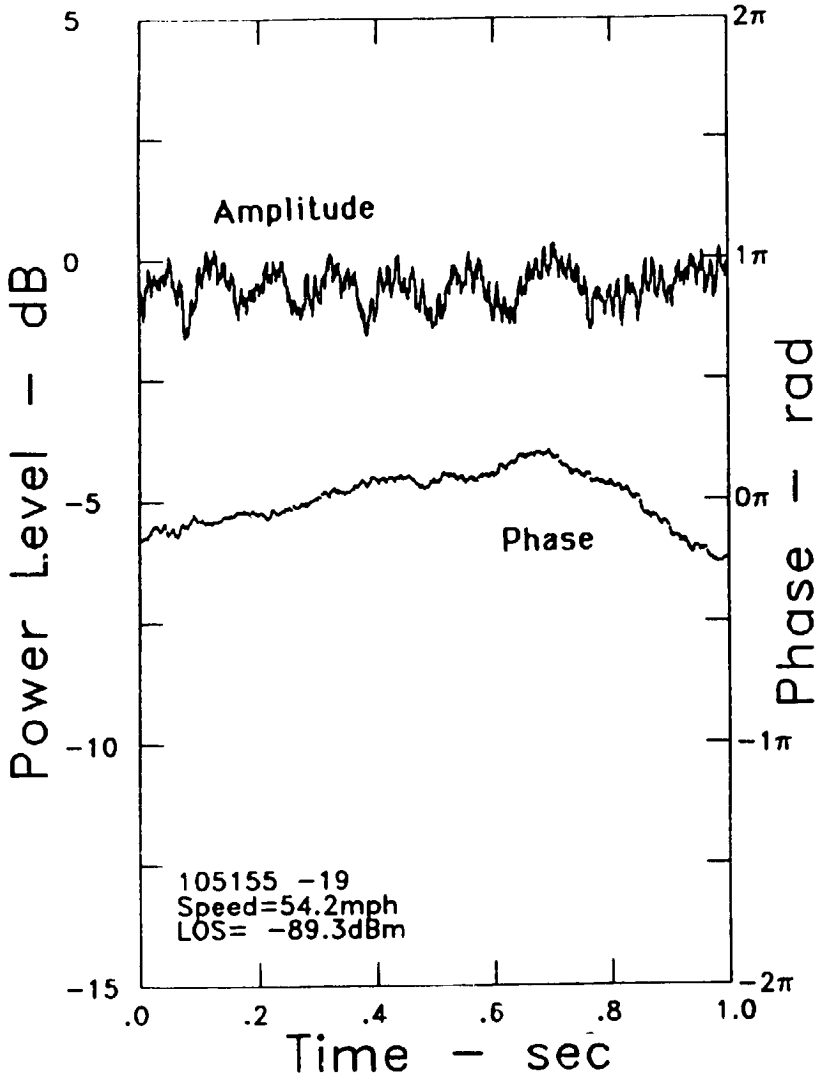

FIG. 8d The beat frequency decreases further, with reduced amplitude. This kind of behavior can be explained by assuming that there were dominant scatterers present; part of the overpass structure or the concrete embankment, for instance.

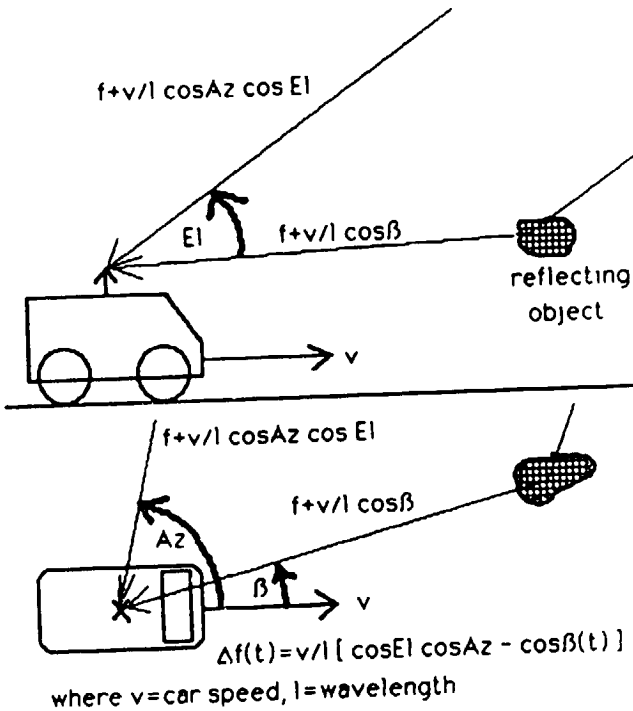

FIG. 9 When a dominant scatterer is present, it sets up an interference beat frequency. As the direction from the vehicle to the scatterer changes, so does the frequency of the beat, because the doppler frequency of the interfering wave changes.

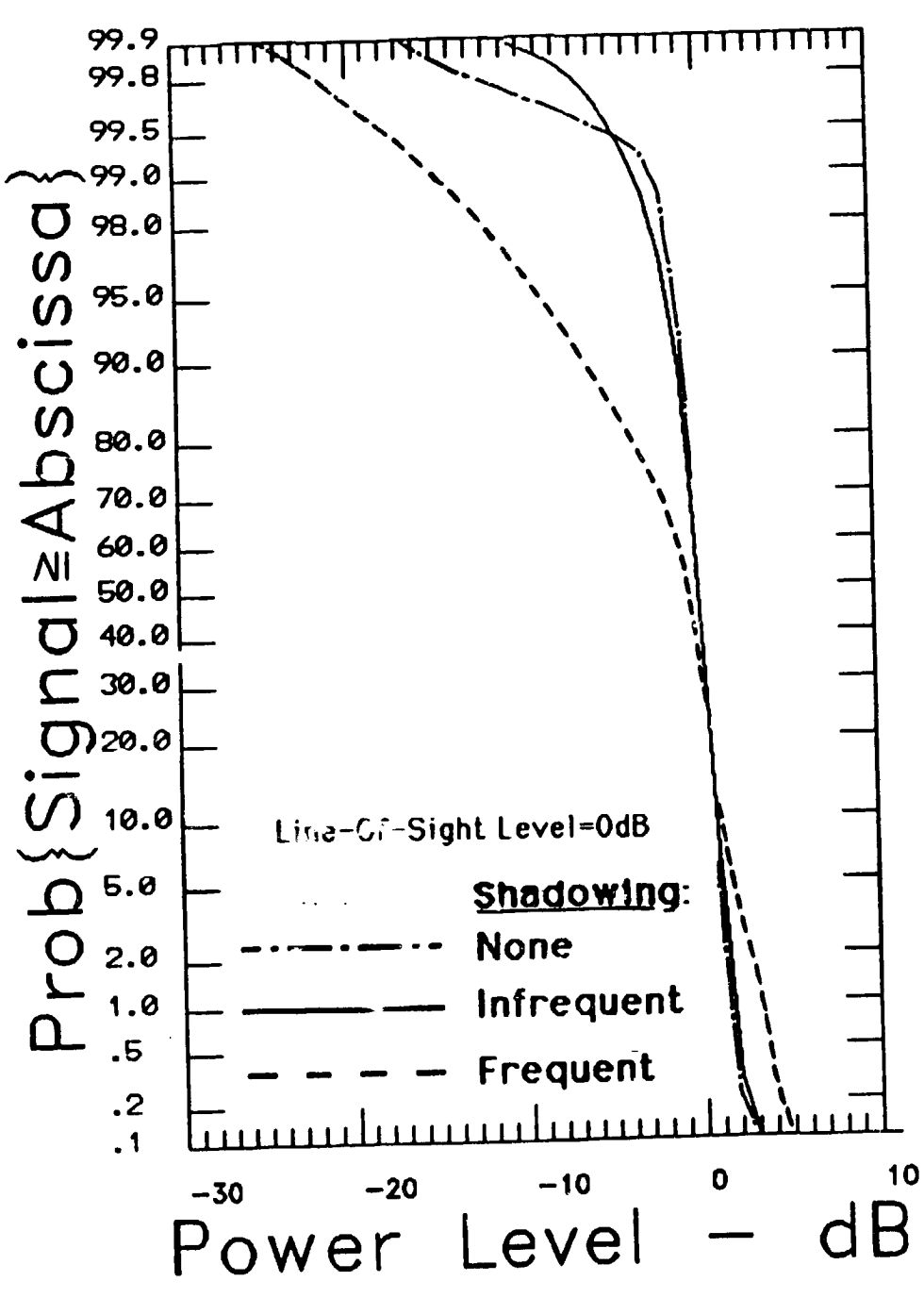

FIG. 10 The power distribution functions for the three cases of no, infrequent, and frequent shadowing give the probability that the signal level was observed above a certain threshold with respect to the estimated clear line-of-sight level. Up to 99.5% the no-shadowing case has the best performance, but then the frequent overpasses included in these data cause a sharp reduction in power level, even below the infrequently shadowed data.

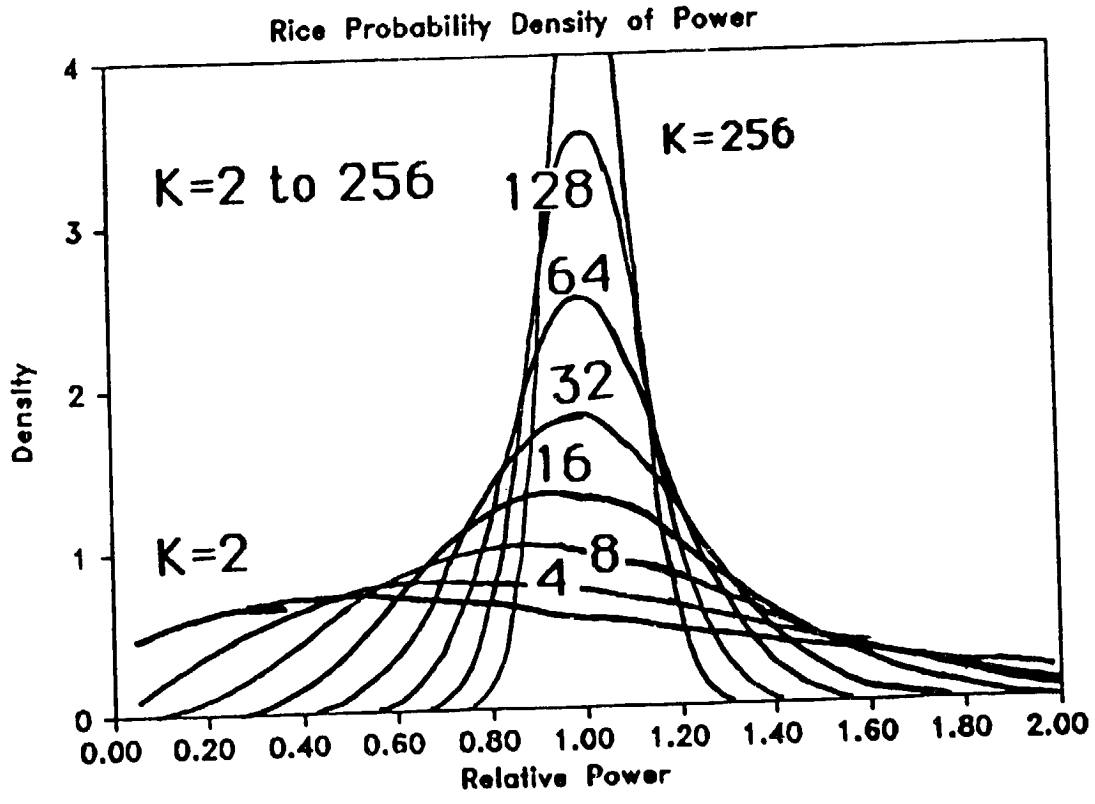

FIG. 11 The probability density function of the power for the Ricean fading case has been plotted for ratios K of the direct to scattered received power from 2 to 256. Ricean fadig is generally assumed to be applicable to the land-mobile satellite case (when there is no shadowing).

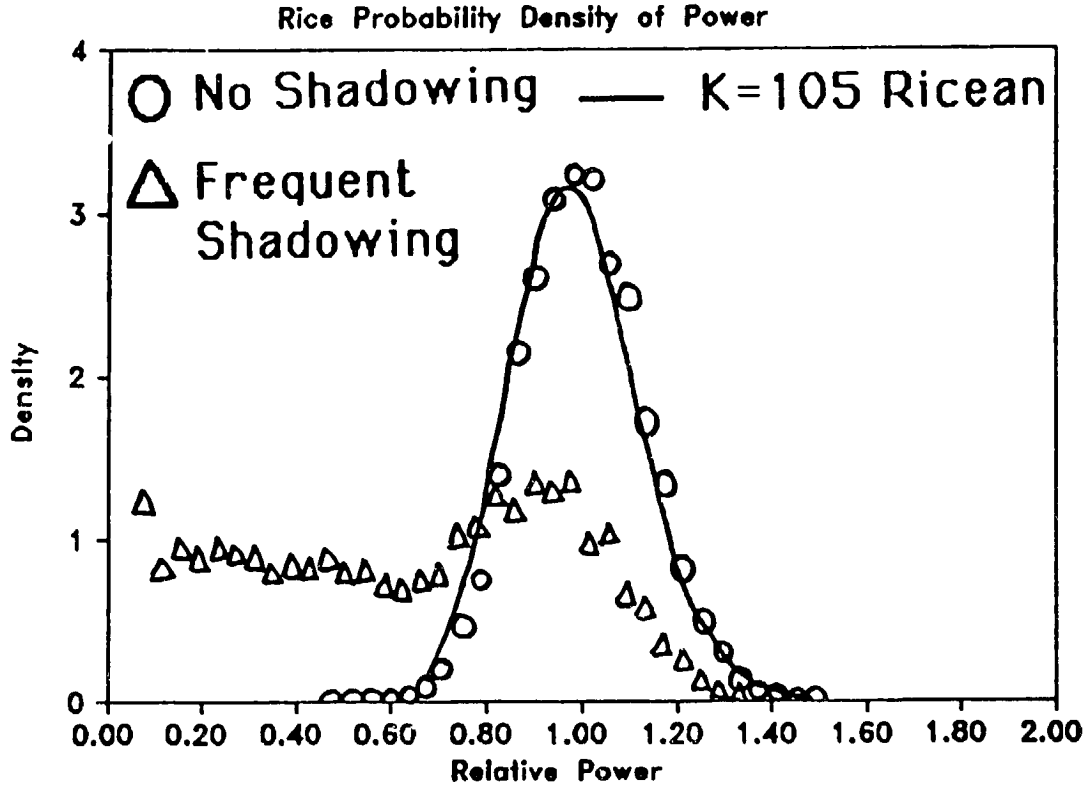

FIG. 11b The circles represent one minute of data observed at 11:51:55 CST, as the van was driving east on IH20 in Mississippi. The triangles show data from the minute starting at 13:35:41 CST, while the line-of-sight to the balloon was shadowed by roadside trees. A Chi-squared goodness-of-fit test was performed on the unshadowed data. The best fit was for K=105, i.e. the scattered power was 20.2 dB below the direct power. The shadowed data are clearly not Ricean, so no fit was performed.

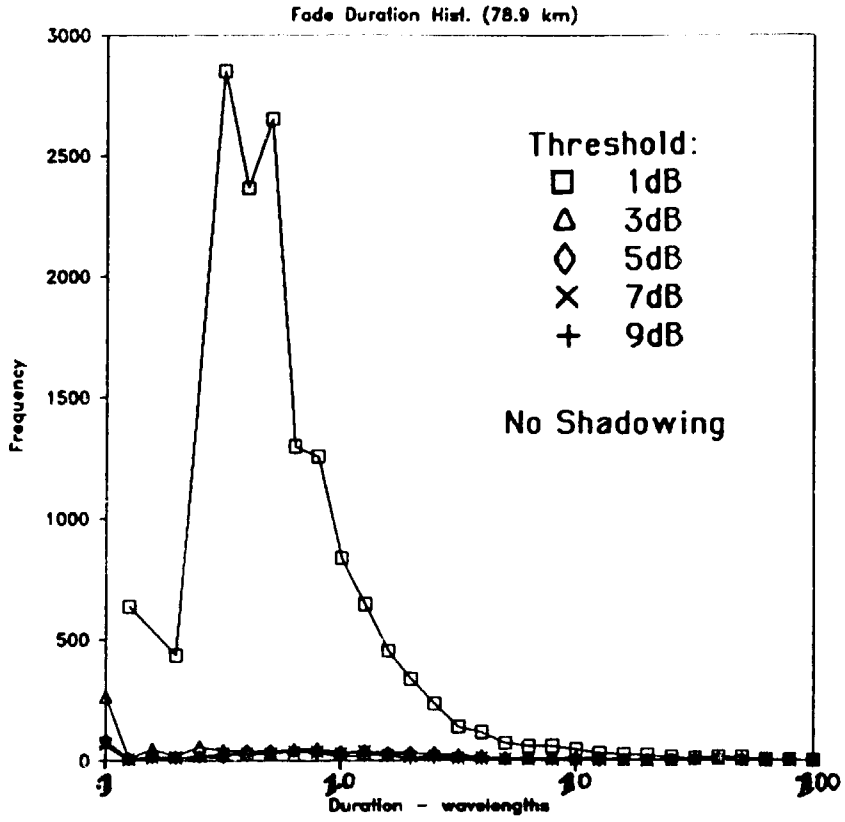

FIG. 12a The fade duration histogram shows the durations of fades and their frequency of ocurrence. In the no-shadowing case few of the fades reached 3dB or more with respect to the LOS level. Most of the 1 dB fade durations were about 1/2 wavelength long.

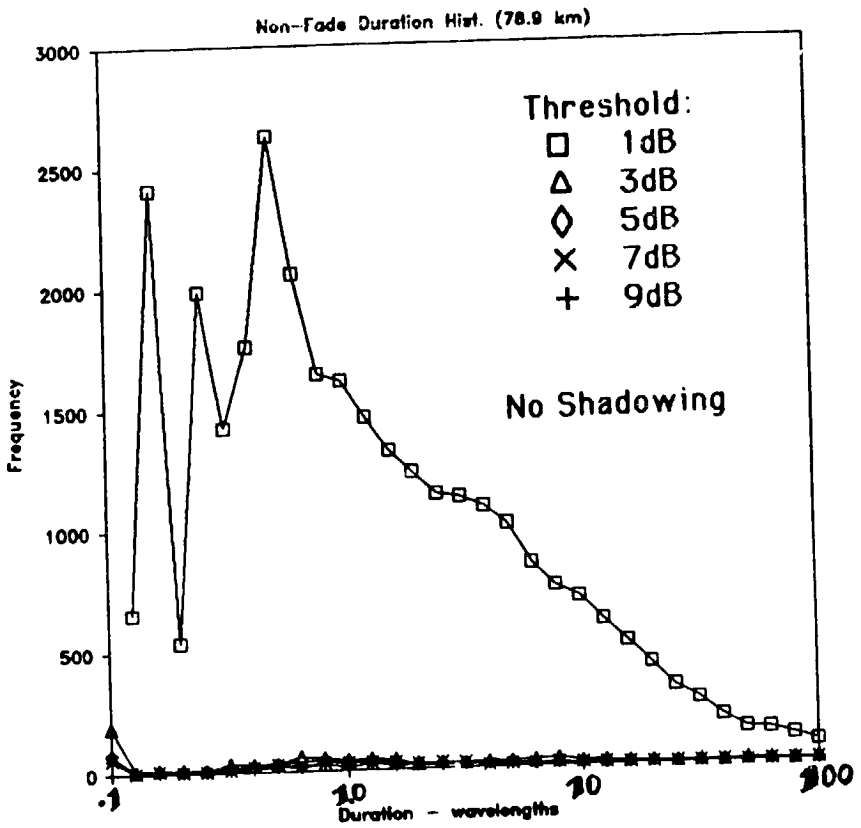

FIG. 12b The duration histogram for the duration of the non-fades, i.e. periods the signal was above the threshold level, is shown, again for non-shadowing data. The jagged appearance at low durations is due to sampling quantization. The non-fade durations were spread out over a wider range than the fade durations.

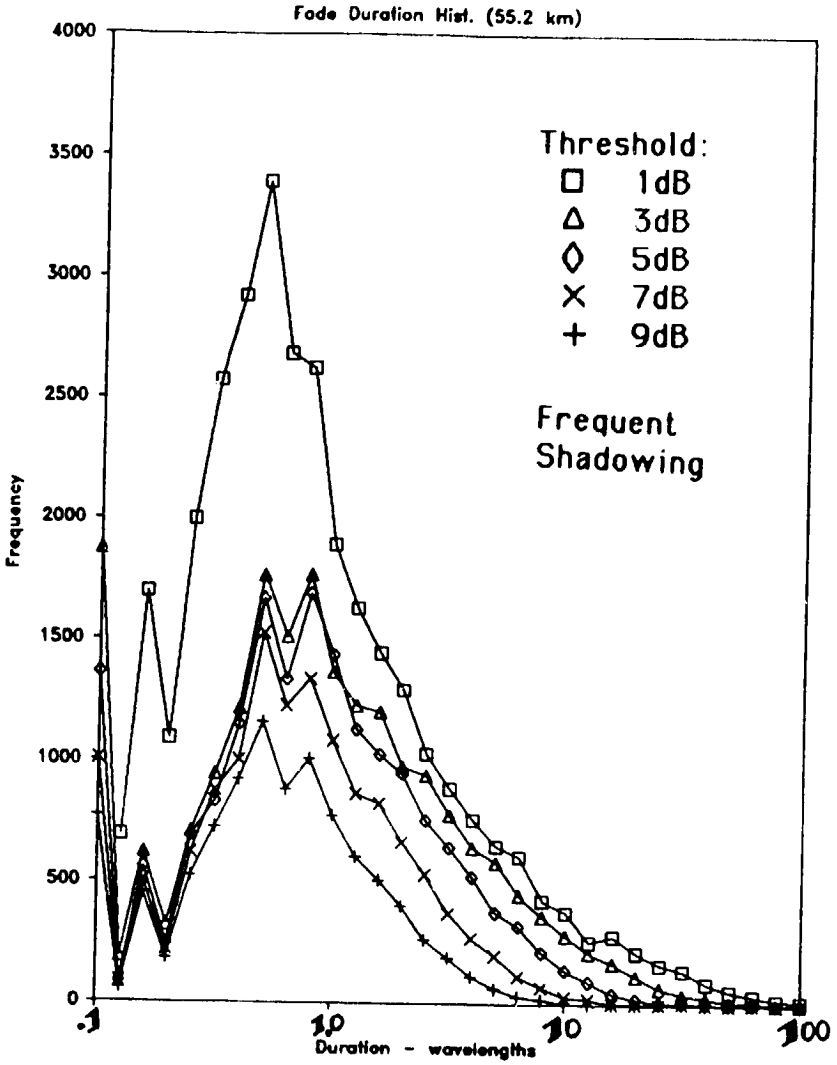

FIG. 12c For the data with frequent shadowing, the fade duration histogram for thresholds of 1, 3, 5, 7, and 9 dB is shown. The most probable fade duration was less than one wavelength.

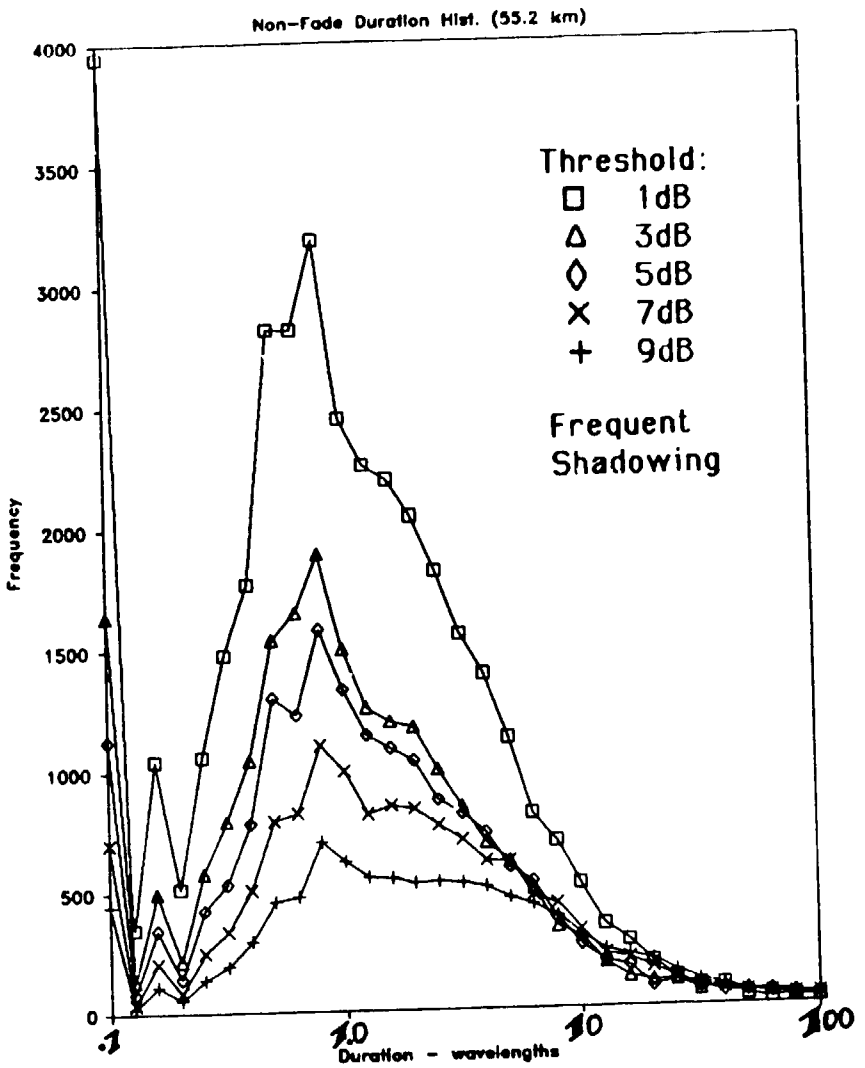

FIG. 12d The frequent shadowing data duration histogram of the non-fades is shown for 1, 3, 5, 7, and 9 dB thresholds. The non-fade durations, especially for the deeper fades, are somewhat more spread out over the .5 to 10 wavelength range.

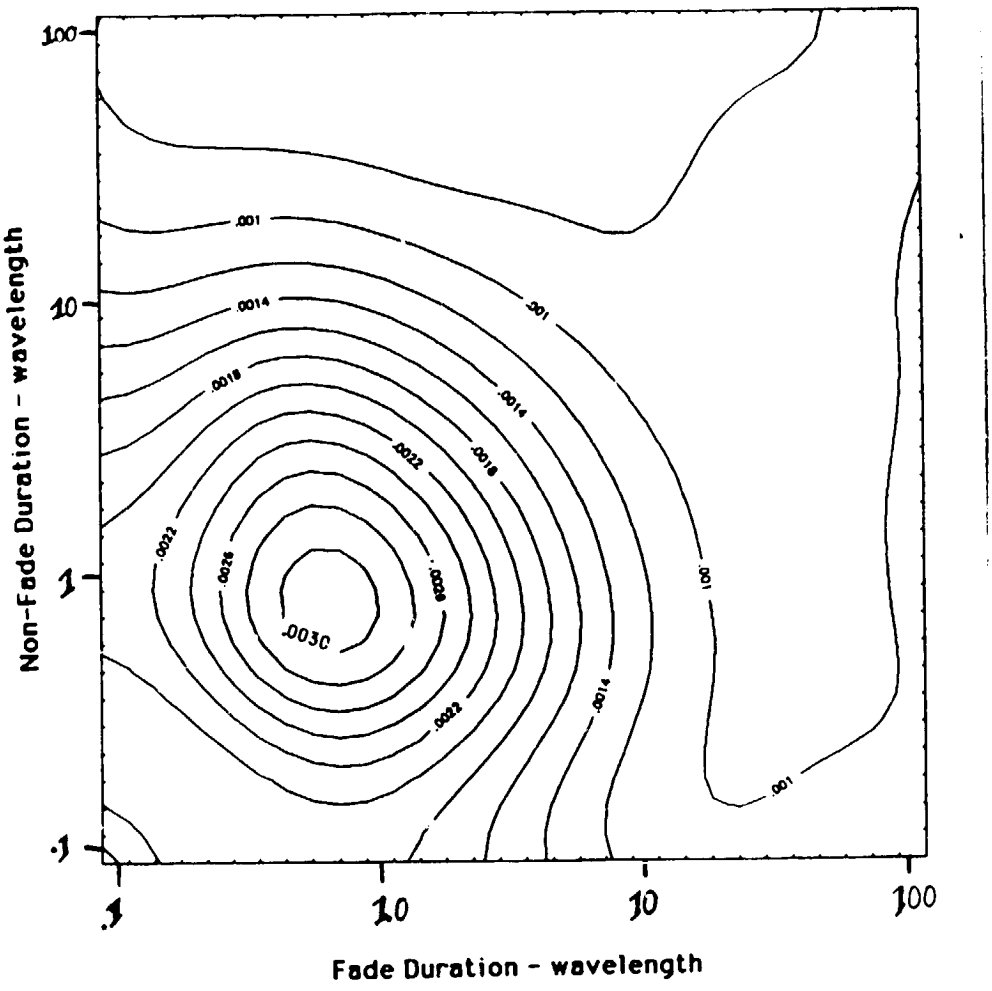

5 dB Level Fade/Non-fade Pair Density, frequent fading

FIG. 13 Fades are always followed by non-fades. One can therefore derive the statistics for the duration of the fade/non-fade pairs. The density function for the 5 dB threshold level and for the data with frequent shadowing is shown here. The contour levels give the fraction of the total of 17,309 pairs observed at a particular fade/non-fade duration combination. One can see that durations just below one wavelength were prevalent. Without hysteresis in the threshold, this result is dominated by the small amplitude ripple of the data.

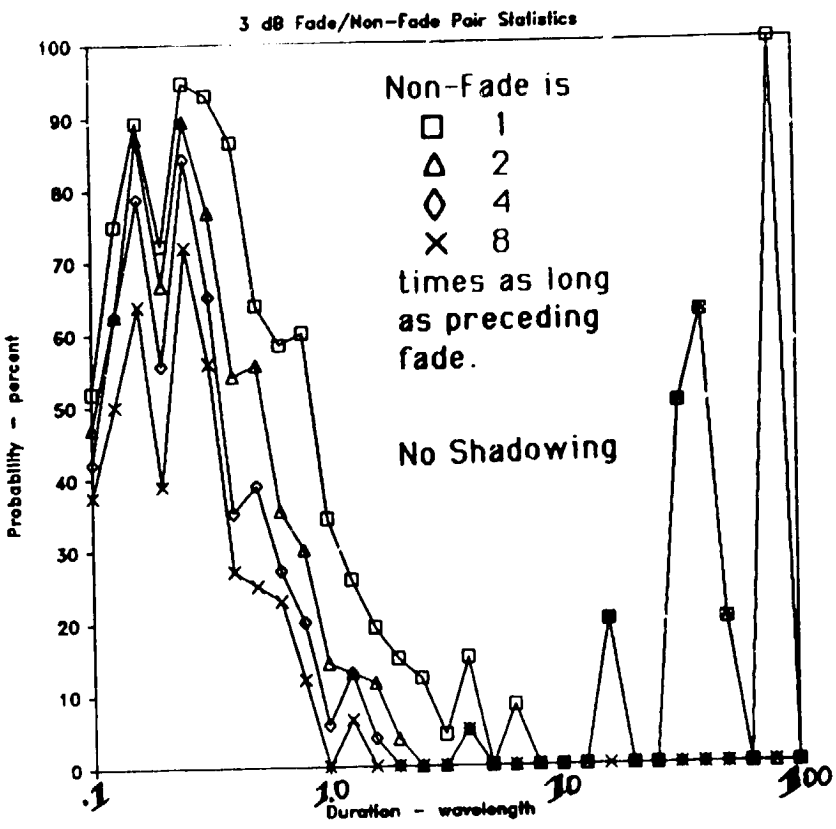

FIG. 14a Shown are the probabilities that a fade is followed by a non-fade of 1, 2, 4, or 8 times the duration of the fade for the no shadowing data and the 3 dB threshold.

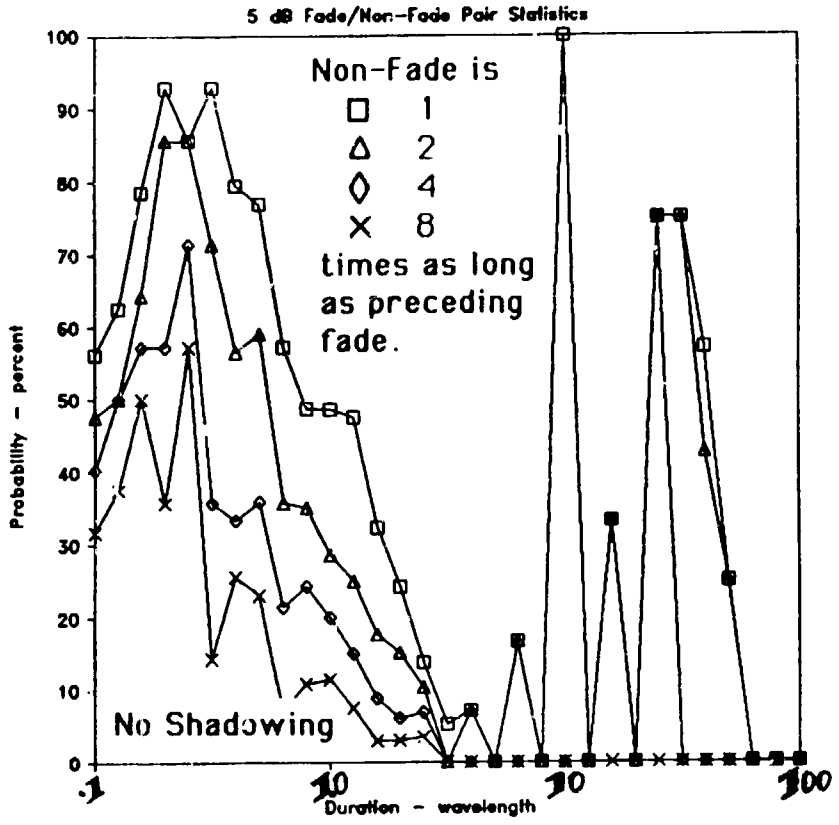

FIG. 14b Probabilities that a fade is followed by a non-fade of 1, 2, 4, or 8 times the duration of the fade for the no shadowing data and the 5 dB threshold are similar to the previous ones. The peaks at the higher durations are due to overpasses.

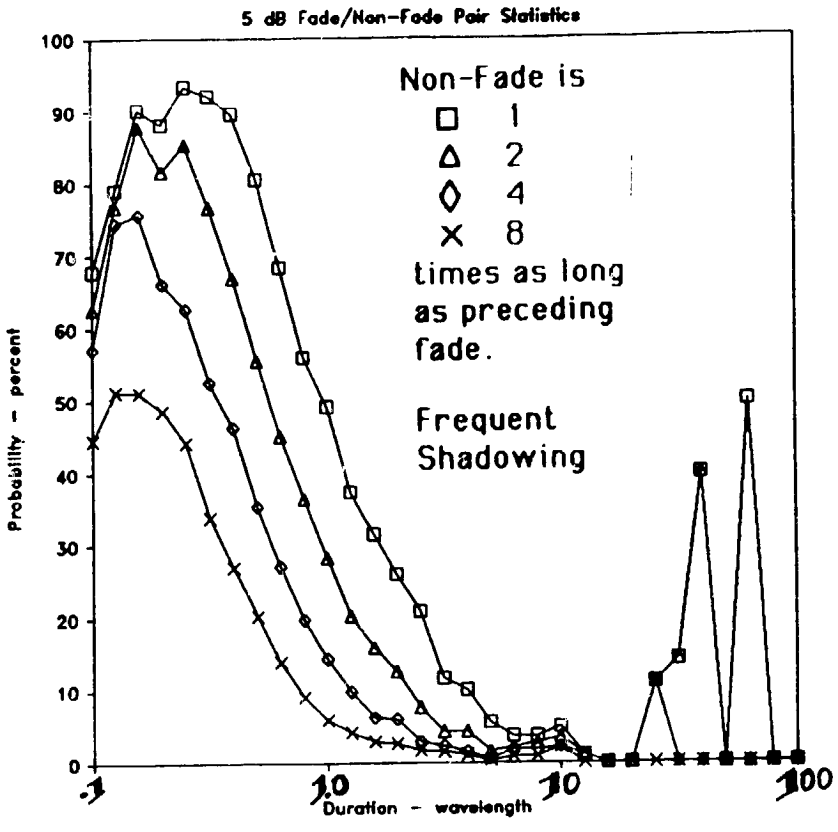

FIG. 14c For the frequent shadowing data given are the probabilities that a fade of a certain duration will be followed by a fade of the same, 2, 4, or 8 times that duration. The threshold for this plot was 5 dB.

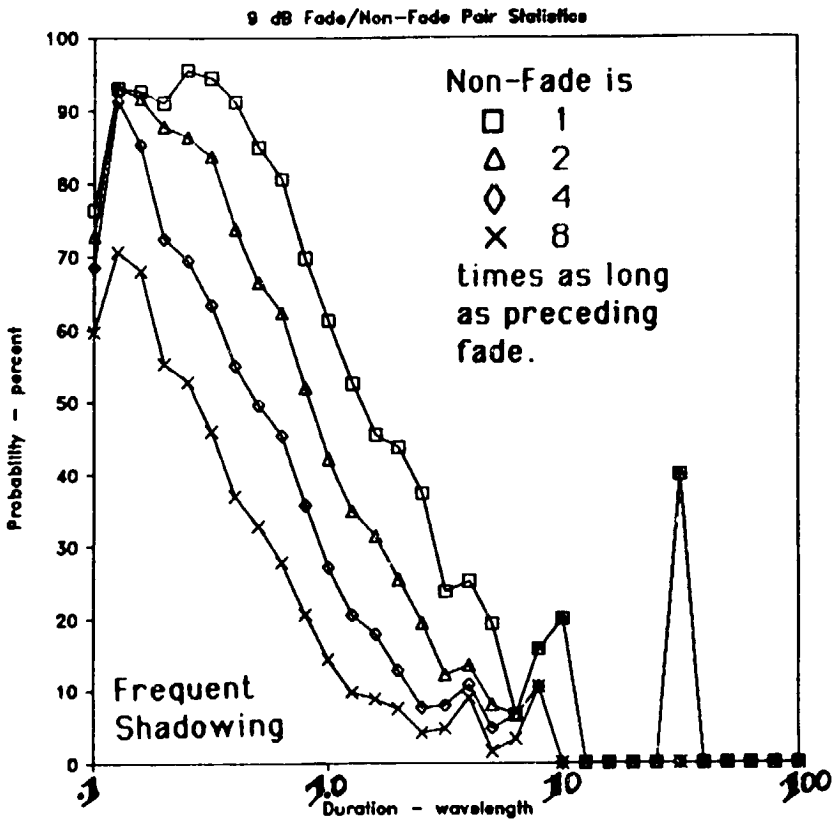

FIG. 14d For the frequent shadowing data given are the probabilities that a fade of a certain duration will be followed by a fade of the same, 2, 4, or 8 times that duration. The threshold for this plot was 9 dB.

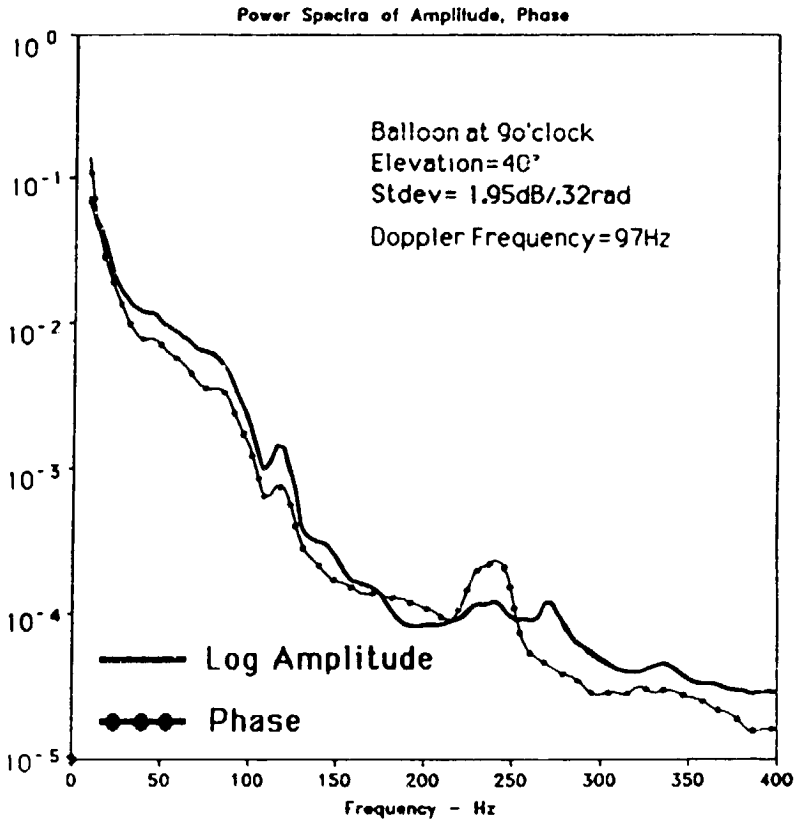

FIG. 15a A normalized power spectrum calculated for the log amplitude and the phase for 63 seconds of data from the frequent shadowing class is shown. The frequency scale has been normalized so that data taken at different van speeds could be averaged. The doppler frequency is 93 Hz for this scale. Most of the power in both the phase and amplitude is below the doppler frequency in this case.

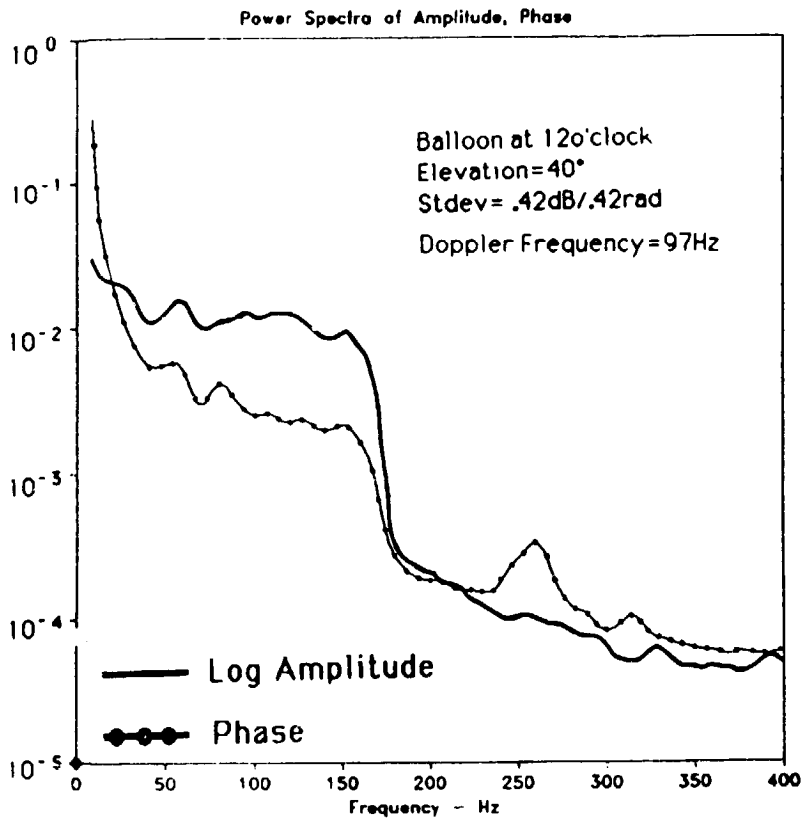

FIG. 15b Data from the non shadowing class show a steep decline in fluctuation power at below about twice the doppler frequency. Theoretically, one would expect scattering contributions to have frequencies within that limit. The shape of the log amplitude and the phase spectra is very similar, except close to zero frequency, where one would expect that frequency instabilities produce slow phase variations.

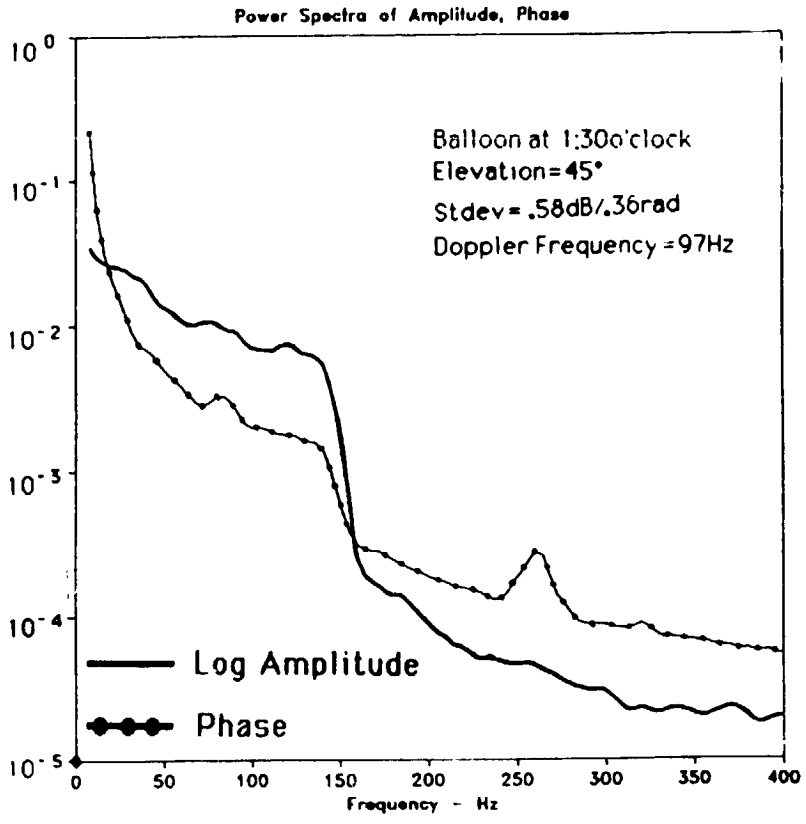

FIG. 15c In this non-shadowing spectrum, the frequency at which the power decreases sharply is lower than in the precious one. This could be explained by the fact that in the previous case the balloon was straight ahead from the van, whereas in this case it was more to the side. The reason for the peak in the phase spectra at about 250 Hz is not known.